UNDERSTANDING THE EFFECT OF SIZING AND CELLULOSE NANOCRYSTALS ON S2 GLASS FIBER SHEET MOLDING COMPOUNDS

A Dissertation
Presented to
The Academic Faculty

by

Hattem Mohammed Hamad Alhuwaimel

In Partial Fulfillment
of the Requirements for the Degree
Master of Science in Materials Science and Engineering
School of Materials Science and Engineering

Georgia Institute of Technology
December 2021

UNDERSTANDING THE EFFECT OF SIZING AND CELLULOSE NANOCRYSTALS ON S2 GLASS FIBER SHEET MOLDING COMPOUNDS

Approved by:

Dr. Kyriaki Kalaitzidou, Advisor
School of Mechanical Engineering
Georgia Institute of Technology

Dr. Robert Moon
Forest Products Laboratory
USDA-Forest Service
School of Materials Science and Engineering
Georgia Institute of Technology

Dr. Donggang Yao
School of Materials Science and Engineering
Georgia Institute of Technology

Date Approved: December 2, 2021

To my parents and siblings.

ACKNOWLEDGEMENTS

I would like to start off by acknowledging the financial support I received from SABIC and P^3 Nano. I would like to also express special thanks and gratitude to my research advisor, Dr. Kyriaki Kalaitzidou, for her continuous support and encouraging mentorship. She helped me when I hit roadblocks, guided me when the course of action was unclear, and encouraged when hope seemed lost. I would also like to thank Dr. Robert Moon for his regularly provided insights that were instrumental in improving my core competency as a scientist. Dr. Kalaitzidou and Dr. Moon successfully fostered a collaborative environment that helped enrich my experience at Georgia Tech. I would also like to thank Dr. Jonathan Colton for providing equipment access, training, and guidance. I would also like to thank past members of the Kalaitzidou group, Eddie DiLoreto, Ejaz Haque, and Arielle Berman, for their invaluable help in getting me started on my journey at Georgia Tech. I would also like to thank the current members of the Kalaitzidou group, Luc Le, Jamie Wooding, Annie Pham, Eric Biederman, and Andrew Wu. Luc and Eric's help with DMA testing was especially appreciated. I would also like to thank James Collins for his assistance with impact testing. I would also like to thank the folks at AGY, Tim Collins, Scott Damron, and Craig Homrighausen, for partnering on this project and for conducting tensile, flexural, and matrix burn off tests. Finally, I would like to sincerely thank my family and friends for their support and companionship during my career at Georgia Tech.

TABLE OF CONTENTS

ACKNOWLEDGEMENTS **iv**

LIST OF TABLES **vii**

LIST OF FIGURES **viii**

LIST OF SYMBOLS AND ABBREVIATIONS **xi**

SUMMARY **xii**

CHAPTER 1. Introduction **1**
1.1 Glass Fiber-Reinforced Polymers (GFRPs) **2**
1.1.1 Thermoset Matrix Composites 2
1.1.2 Glass Fibers 3
1.1.3 Sizing 5
1.1.4 Cellulose Nanomaterials (CNMs) 6
1.2 Sheet Molding Compounds (SMC) Technology **9**
1.2.1 General SMC Background 10
1.2.2 Compression Molding 12
1.3 Goal and Objectives **13**

CHAPTER 2. Materials and Methods **16**
2.1 Materials **16**
2.1.1 Resin 16
2.1.2 Reinforcement and Additives 17
2.2 Manufacturing and Fabrication **17**
2.2.1 Resin Preparation 17
2.2.2 Fabrication of SMC 18
2.2.3 Compression Molding 20
2.2.4 Testing Coupons Preparation 21
2.3 Characterization Techniques **21**
2.3.1 Microscopy 21
2.3.2 Mechanical Testing 21
2.3.3 Density Measurements 23
2.3.4 Determination of Constituent Content 23
2.3.5 Viscoelastic Properties 24
2.3.6 Thermal Transitions 25
2.3.7 Glass Fiber Surface Analysis 25

CHAPTER 3. UNDERSTANDING THE EFFECT OF S2 GLASS FIBERS SIZING ON THE MECHANICAL PROPERTIES OF S2 GLASS FIBER/POLYESTER COMPOSITES **26**
3.1 Morphology of S2 GF Sizing **26**
3.2 Density, Glass and Void Content **27**

3.3 Mechanical Properties (Tensile, Flexural, and Impact) 28
3.4 Thermomechanical Properties 32
3.5 Glass Fiber Surface Analysis 36

CHAPTER 4. UNDERSTANDING THE EFFECT OF CELLULOSE NANOCRYSTALS ON THE MECHANICAL PROPERTIES OF S2 GLASS FIBER/POLYESTER COMPOSITES 41
4.1 Introduction 41
4.2 CNC Dispersion 41
4.3 Density, Glass and Void Content 42
4.4 Mechanical Properties (Tensile, Flexural, and Impact) 44
4.5 Thermomechanical Properties 50

CHAPTER 5. Conclusions and Future Work 55
5.1 Conclusions 55
5.2 Future Work 57

REFERENCES 59

LIST OF TABLES

Table 1-1	Properties of thermosets commonly used in composites [8].	4
Table 1-2	Properties of fibers commonly used in reinforcing composites [8, 11].	4
Table 1-3	Components of a typical SMC material [46].	11
Table 1-4	Typical properties of SMC (Polyester resin, $CaCO_3$ filler, and 25 wt% E-glass fibers) [13].	12
Table 1-5	Overview of the research plan.	15
Table 2-1	Resin formulation details used throughout the project.	16
Table 3-1	Experimental and theoretical density, void, and GF content of the S2-GF/ polyester SMC composites as a function of the CNC content.	27
Table 3-2	Viscoelastic properties of composites made with differently sized S2-GF obtained from 3-point-bending DMA tests.	35
Table 3-3	Numerical description of carbon bonding within the glass fiber sizing as obtained from XPS C1s spectra.	36
Table 3-4	Atomic% of C, O, Si, and Al for the different S2-GF samples. Obtained from XPS Spectra.	37
Table 4-1	Experimental and theoretical density, void and GF content of the E-GF and S2-GF/ polyester SMC composites as a function of the CNC content.	43
Table 4-2	Viscoelastic properties of the five different E-GF/polyester and S2-GF/polyester SMC composites as a function of the glass fiber type and CNC content. Obtained from DMA 3-point-bending DMA tests.	54

LIST OF FIGURES

Figure 1-1	A schematic picture of the sizing applicator alongside a photo from a glass fiber production line [16].	6
Figure 1-2	Transmission electron microscopy (TEM) images of dried dispersion of CNMs from different sources: a) CNCs [35], b) CNF with fibrillation pretreatment [36], c) CNF without fibrillation pretreatment [37], d) tunicate CNCs [38], e) AC [37], and f) Scanning electron microscopy (SEM) image of BC [39].	8
Figure 1-3	A flowchart describing the process of making SMC composites [45].	10
Figure 1-4	A schematic showing different SMC products [47].	11
Figure 1-5	A schematic of a typical compression molding process [46].	13
Figure 2-1	A picture of the Finn and Fram SMC line used in this work [45].	19
Figure 2-2	A simplified diagram of a typical SMC line.	20
Figure 3-1	SEM Images of S2 glass fibers with the three different sizing formulations.	26
Figure 3-2	Tensile strength and modulus of S2-GF/polyester SMC composites as a function of the S2-GF sizing. Results are normalized with respect to the strength and modulus of the 0S2R composite to comply with AGY's corporate practices.	30
Figure 3-3	Flexural strength and modulus of S2-GF/polyester SMC composites as a function of the S2-GF sizing. Results are normalized with respect to the strength and modulus of the 0S2R composite to comply with AGY's corporate practices.	31
Figure 3-4	Impact strength for notched and unnotched S2-GF/polyester SMC composites as a function of the S2-GF sizing. Impact energy absorbed by the coupon was divided by the cross-section and reported in J/cm^2.	32
Figure 3-5	Glassy and rubbery modulus values of the three different S2-GF/polyester SMC composites as a function of the S2 GF sizing. Obtained from 3-point-bending DMA tests.	33

Figure 3-6	The area under the curve of the tan δ peak of the three different S2-GF/polyester SMC composites as a function of the S2 GF sizing. Integration was done from 50°C degrees below the tan δ peak maximum to 50°C degrees above the tan δ peak maximum. Obtained from 3-point-bending DMA tests.	34
Figure 3-7	DSC curves of three S2-GF samples with different sizing formulations. Heating rate was 10 °C/min. T_g of polymeric film of the sizing was not noted.	35
Figure 3-8	C1s XPS of S2-GFs with different sizing formulations.	36
Figure 3-9	Atomic% of C, O, Si, and Al for the different S2-GF samples as a function of sizing.	38
Figure 3-10	Possible sizing arrangements. a) thick uniform sizing with moderate functional group density. b) thin uniform sizing with moderate functional group density. c) erratic sizing with moderate functional group density. d) thick uniform sizing with high functional group density. e) thin uniform sizing with high functional group density. f) erratic sizing with high functional group density.	39
Figure 4-1	SEM images of S2P composites as a function of CNC content: 0 PHR (left), 2.5 PHR (center) and 5 PHR (right).	42
Figure 4-2	Tensile strength and modulus of E-GF/polyester and S2-GF/polyester SMC composites as a function of fiber type and CNC content. Results are normalized with respect to the strength and modulus of the 0E composite to comply with AGY's corporate practices.	45
Figure 4-3	Flexural strength and modulus of E-GF/polyester and S2-GF/polyester SMC composites as a function of fiber type and CNC content. Results are normalized with respect to the strength and modulus of the 0E composite to comply with AGY's corporate practices.	46
Figure 4-4	Impact strength for notched and unnotched E-GF/polyester and S2-GF/polyester SMC composites as a function of fiber type and CNC content. Impact energy absorbed by the coupon was divided by the cross-section and reported in J/cm^2.	47
Figure 4-5	Predicted values of the elastic modulus of E-GF/polyester and S2-GF/polyester composites as a function of fiber type and CNC content. Results are normalized with respect to the modulus of the 0E composite. Obtained using the Halpin-Tsai and E_{random} equations.Figure 4-5: Predicted values of the elastic	50

modulus of E-GF/polyester and S2-GF/polyester composites as a function of fiber type and CNC content. Results are normalized with respect to the modulus of the 0E composite. Obtained using the Halpin-Tsai and E_{random} equations.

Figure 4-6 Glassy and rubbery modulus values of the 5 different E-GF/polyester and S2-GF/polyester SMC composites as a function of glass fiber type and CNC content. No clear trend observed. 51

Figure 4-7 Normalized glassy and rubbery modulus values of the five different E-GF/polyester and S2-GF/polyester SMC composites as a function of glass fiber type and CNC content. Modulus decreased proportionally with the addition of CNCs without statistical significance. 53

Figure 4-8 T_g, temperature at tan δ maximum, as obtained from 3-point-bending DMA tests of the five different E-GF/polyester and S2-GF/polyester SMC composites as a function of the glass fiber type and CNC content. 54

LIST OF SYMBOLS AND ABBREVIATIONS

AC	Algal Cellulose
BC	Bacterial Cellulose
CMS	Cellulose Microfibrils
CNCs	Cellulose Nanocrystals
CNFs	Cellulose Nanofibrils
CNMs	Cellulose Nanomaterials
DMA	Dynamic Mechanical Analysis
DSC	Differential Scanning Calorimetry
ESCA	Electron Spectroscopy for Chemical Analysis
FRCs	Fiber-reinforced Composites
FRPs	Fiber-reinforced Polymers
GF	Glass Fiber
GFRP	Glass Fiber-Reinforced Polymer
NCC	Nanocrystalline Cellulose
NFC	Nanofibrillated Cellulose
PHR	Parts per Hundred Resin
SEM	Scanning Electron Microscopy
SMC	Sheet Molding Compounds
TEM	Transmission Electron Microscopy
XPS	X-Ray Photoelectron Spectroscopy

SUMMARY

Glass Fiber Reinforced Polymers (GFRPs) are increasingly more ubiquitous as research continuously pushes the limits of their mechanical performance. Excellent mechanical properties and low density coupled with increased ease of processibility are what distinguishes GFRPs over metallic materials. Emphasis has been given mainly to E-glass fibers as their low cost drove their demand. This work focuses on the more structurally graded S2-glass fibers which still are not performing as carbon fibers in terms of modulus, strength, or density, but they are seen as an alternative to E-glass fibers when carbon fibers are not an option. The question of interest is whether the performance of S2 glass fibers structural composites has reached its plateau or if there is still opportunity for improvement. This work seeks to investigative the potential of modifying glass fiber surface finish (sizing), and the addition of cellulose nanocrystals (CNCs) to improve the mechanical properties of S2-GFRPs. S2-GF/polyester SMC composites with three different types of glass fiber sizing were compared in terms of tensile, flexural and impact properties. The three types of sizing were characterized microscopically and using spectroscopic techniques, and differences in their chemistry (functional groups) were investigated. It was found that the tensile and flexural strength increased with increased conformability of the sizing film on the fibers, with the most conforming sizing resulting in composites with around 30% improvement in tensile and flexural strength, followed by the second best which exhibited around 20% improvement in tensile and flexural modulus, over the composite with the less conforming sizing film. No significant differences in the functional groups of the sizings were identified. This behavior is

attributed to the enhanced interfacial interactions between the sizing and the fiber surface in the more conforming sizing films. The effect of CNCs on the mechanical properties of S2-GFRPs was marginal. However, the T_g of the composite increased ~ 6°C with the addition of 5 PHR CNCs due to the nanoparticles restricting the matrix polymer chains, and this was indicative of increased thermal stability in S2-GFRPs.

CHAPTER 1. INTRODUCTION

Fiber-Reinforced Polymers (FRPs), first introduced in the late 1930s [1], are increasingly replacing metallic parts as they have excellent mechanical properties and increased processibility. In fact, with proper selection of matrix and fibers, one can manufacture a polymer composite with strength and modulus that are comparable to many metallic materials. Composites generally possess superior specific strength to that of metals [2]. In the automotive and marine industries, for example, FRPs with 30-50 wt% short fibers are commonly used for their stiffness and high specific strength [3]. The use of FRPs has the potential to improve fuel efficiency in vehicles, as a 10% reduction in a vehicle's mass can lead to a 6%-8% reduction in the vehicle fuel consumption [4]. This push for improved fuel efficiency is driven in part by regulations that seek to reduce fuel consumption and emissions [5]. Consequently, many automotive manufacturers have been interested in lightweight materials.

Lightweighting is the practice of improving the properties of a given part so that a lighter part could be used to serve the purpose without any loss in function. One of the challenges with lightweighting is related to property tradeoff. That is, an increase in one property is often accompanied with a decrease in another property. For example, increasing the strength or stiffness, commonly done by modifying the fibrous reinforcements or the introduction of non-fibrous reinforcements, is oftentimes coupled with a decrease in impact strength [6]. Glass fibers are coated with a thin film called sizing, and cellulose nanocrystals (CNCs) are bio-sourced crystalline particles with unique properties. This work seeks to explore the possibility of holistically improving the

mechanical properties of Glass Fiber Reinforced Polymers (GFRPs) through exploring the potential of glass fiber sizing and CNCs.

Interest in cellulose nanocrystals (CNCs) can be gauged by the upward slope in the number of publications dedicated to them: in 2020 alone, about 2000 studies discussing CNCs were published [7]. This interest comes, in part, from the sustainable nature and excellent structure and properties of CNCs. Additionally, CNCs' high aspect ratio allows them to proficiently facilitate load transfer within a composite—thus making CNCs an ideal solution for lightweighting.

Many studies investigated the effect of CNCs on GFRPs, but they are mostly focused on E-glass fibers. This work seeks to explore CNCs' effect on GFRPs containing structurally graded S2 glass fibers. S2-GF have higher tensile strength and modulus than E-GF, and therefore are more suitable for structural applications. In addition to exploring the effect of CNCs on S2 GFRPs, this work also seeks to examine the potential of glass fiber sizing by examining GFRPs that use S2 glass fibers with different surface chemistries to improve our understanding regarding the potential of the glass fiber sizing. This work is done with GFRPs that are manufactured using Sheet Molding Compounds (SMC) technology.

1.1 Glass Fiber-Reinforced Polymers (GFRPs)

1.1.1 Thermoset Matrix Composites

Thermoset-matrix composites are commonly used in many industries including aerospace, automotive, and electronics. One main reason thermosets are more popular than thermoplastics is their much lower viscosity, which facilitates processability and

better wetting of the fibers leading to an increase in the stress transfer ability across the fiber-matrix interface, which results in increased strength and stiffness of the composite. Additionally, thermosets have higher heat and chemical resistance than thermoplastics, and they are less susceptible to creep deformation. Limitations of thermosets include longer processing times compared to thermoplastics. Lastly, it's worth noting that thermosets cannot be remelted, and this limits reuse and recyclability [8]. Thermosets are generally made by reacting liquid pre-polymers in the presence of a catalyst. Polymerization then happens and the liquid pre-polymers undergo cross-linking, resulting is a solidified polymer [8].

Polyesters present a sizable portion of thermosets and are commonly used in composites due to their good mechanical properties, low cost, and fast cure time [9]. Polyesters generally come in two types depending on the isomer used for the preparation of the resin. Orthophthalic polyester is for more general-purpose use and is more widely used than isophthalic polyester. However, isophthalic polyester possesses superior strength, crack resistance and chemical resistance properties [10]. Polyesters, vinyl esters, and epoxies are the most widely used thermosets. The coupling agents in the sizing of the S2-GF being investigated in this work had compatibility with polyesters and vinyl esters. Polyester resin was chosen for this work for its low cost and somewhat comparable properties to vinyl esters. Table 1-1 lists a brief comparison between the properties of the most popular thermosets.

1.1.2 Glass Fibers

Fibers play a crucial role in polymer composites as they are the main load carrier constituent. Fiber characteristics that strongly influence the properties of the composite

include fiber aspect ratio, fiber type (glass, carbon, etc.), and fiber amount (often reported as vol%). Table 1-2 below presents some of the properties of the fibers most used in composites.

Table 1-1: Properties of thermosets commonly used in composites [8].

Polymer	Density (g/cm^3)	Tensile Strength (MPa)	Tensile Modulus (GPa)	Strain at Failure (%)
Polyesters	1.1-1.43	34.5-103.5	2.1-3.45	1-5
Vinyl esters	1.12-1.32	73-81	3-3.5	3.5-5.5
Epoxies	1.2-1.3	55-130	2.75-4.10	-

Table 1-2: Properties of fibers commonly used in reinforcing composites [8, 11].

Fiber Type	Density (g/cm^3)	Tensile Strength (GPa)	Tensile Modulus (GPa)	Strain at Failure (%)
E-glass	2.54	3.45	72.4	4.8
S-glass	2.49	4.30	86.9	5.0
S2-glass	2.46	4.89	89.9	5.7
Carbon	1.76-2.15	1.90-5.18	228-758	0.32-1.89
Aramid	1.45	3.62	131	2.8

E-glass fibers are the most used as they possess low cost, high tensile strength, and excellent insulating properties. However, E-glass fibers have higher density and are

highly sensitive to moisture absorption. S-glass fibers (also called structural glass) were originally developed for aerospace and defense applications. S-glass fibers have much higher tensile strength but suffer when it comes to manufacturing—as the process is heavily involved and expensive. S2 glass fibers have very similar properties to that of S glass fibers, but S2 glass fibers have a more straightforward manufacturing process, resulting in a lower cost compared to S-glass [8].

1.1.3 Sizing

Fibers are usually coated with a thin layer of a sizing agent. The sizing agent provides protection to the fibers from any damage they may incur from inter-filament abrasion or from any of the other processing steps the fibers undergo. Additionally, sizing promotes the compatibility between the fibers and the matrix, therefore improving the overall adhesion in the composite and reducing the void content [12, 13]. Shortly after the formation of the fibers from the molten state, the sizing formulation is applied onto the fibers. Fiber sizing has been described as the most critical component in the glass fiber manufacturing process [14], therefore most sizing formulations are proprietary. Commercially available glass fibers are always sized and obtaining unsized fibers is usually accomplished by removing the sizing layer from the as-received fibers by burning off or by soxhlet extraction with acetone [15]. Figure 1-1 shows a schematic of the sizing applicator alongside a photo from a glass fiber production line [16]. FRP composites that are designed for structural applications require a very strong fiber/matrix interface, and this interface is often tuned and improved using the fiber sizing. In fact, some studies showed that in three dimensional GFRP composites, the interphase is largely formed through the interdiffusion of components of the sizing agent [17]. Sizing agents are

usually added to be about 1.4%-1.8% by weight, as measured by ignition loss [18]. The thickness of sizing films ranges from 0.5 to 1.0 μm for glass fibers of diameters 10 to 14 μm. Generally, a sizing agent is made of around 80-90 wt% film former, 5-10 wt% silane coupling agents, and 5-10 wt% auxiliary agents [19]. The purpose of the silane coupling agents is to chemically react with the matrix to form a copolymer, which generally has a favorable influence on the mechanical properties [20].

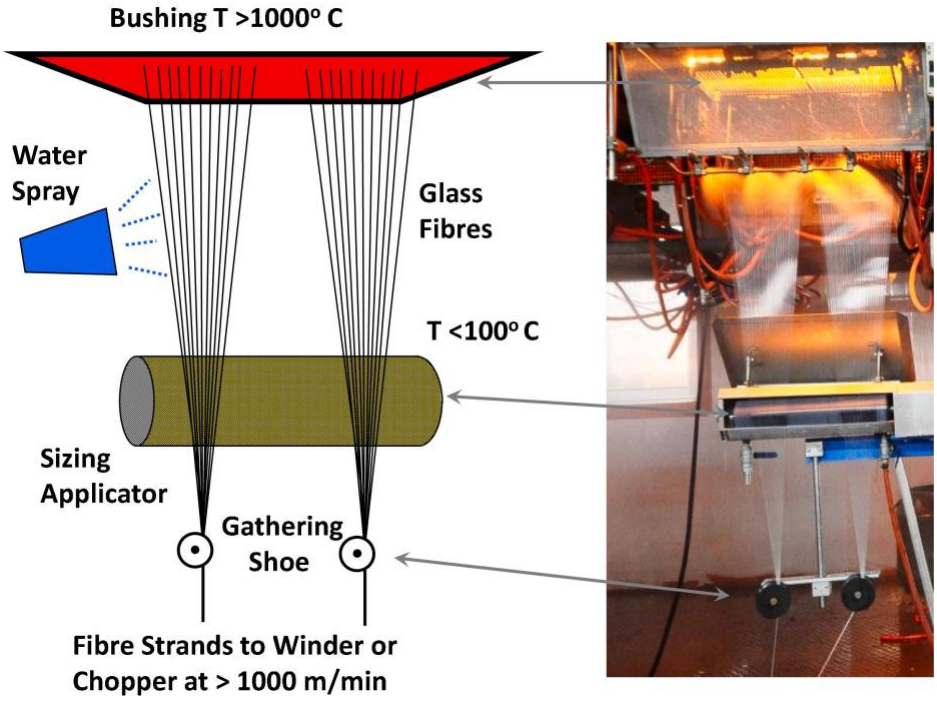

Figure 1-1: A schematic picture of the sizing applicator alongside a photo from a glass fiber production line [16].

1.1.4 Cellulose Nanomaterials (CNMs)

Cellulose is the most common organic polymer on the planet as more than 10^{12} tons are produced each year [21]. Throughout history, many naturally occurring cellulose-based products were utilized by different societies. These natural products

include hemp, linen, cotton, wood, and many others [22]. Demand for cellulose has been on the rise as research and industry interests shift to more environmentally friendly materials. The recent ability to isolate nano-sized cellulose particles, called cellulose nanomaterials (CNMs), from various types of biomass, have resulted in materials that have properties and functionalities that are unique from that of the traditional cellulose materials (e.g., wood, pulp, cellulose derivatives) and thus has created new opportunities for the utilization of cellulose in new application areas. Interest in CNMs is motivated by their unique characteristics, including nano-sized fibril morphology, large surface area, high mechanical properties, shear thinning and thixotropic properties, transparency, sustainability, renewability, and low environmental and health issues [23]. One can glean insights on the breadth of utility of CNMs by noting that they are being researched and utilized for a wide range of applications. These applications include, but are not limited to, biorecognition and imaging [24], barrier/separation membranes [25] [26], adhesives [27], reinforcement of polymers and polymer composites [3] [28] [29], coatings, cements, 3D printing, and cell culturing. CNMs is an umbrella term used to refer to all nanosized cellulose products. The specific type of the CNM depends on cellulose source, extraction and production method, and the surface chemistry. Subsets of CNMs include cellulose nanocrystals (CNCs), cellulose nanofibrils (CNFs), algal cellulose (AC), and bacterial cellulose (BC). Figure 1-2 shows CNMs that have been produced from different sources alongside length scales, which highlight some of the differences among these materials.

This work is chiefly concerned with cellulose nanocrystals (CNCs). CNCs are commonly produced by sulfuric acid hydrolysis, but some CNCs are produced by hydrochloric acid hydrolysis [30] [31] [32]. CNCs are nanosized highly ordered rod-like

particles (often described as whisker shaped) with a generally high aspect ratio. CNCs are about a few nanometers in diameter, and their lengths often range from tens of nanometers to several micrometers [33, 34]. The specific morphology of the CNCs is dictated by the conditions of the acid hydrolysis step and by the source of the cellulose. CNCs produced from wood are 3-5 nm in width and 50-250 nm in length. CNCs produced from a Valonia, a type of algae, have a width of 20 nm and a reported length of 1000-2000 nm. Cotton-based CNCs are 5-10 nm in width, and 100-300 nm in length. CNCs could also be produced from a sea animal, called tunicate, which are reported to be 10-20 nm in width and 500-2000 nm in length. Although high aspect ratio is characteristic of CNCs, one can see that this aspect ratio ranges from 10 to 70 depending on the source [30].

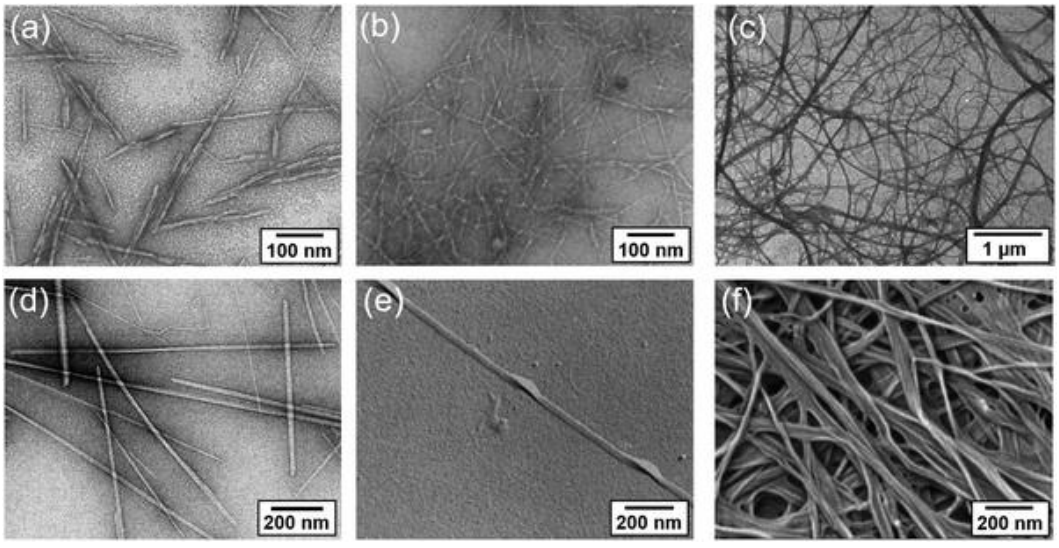

Figure 1-2: Transmission electron microscopy (TEM) images of dried dispersion of CNMs from different sources: a) CNCs [35], b) CNF with fibrillation pretreatment [36], c) CNF without fibrillation pretreatment [37], d) tunicate CNCs [38], e) AC [37], and f) Scanning electron microscopy (SEM) image of BC [39].

In addition to having high aspect ratios, CNCs boast high mechanical properties, low thermal expansion, low density, and surface accessible functional groups that can be readily modified to suit a variety of applications. These generally favourable characteristics have encouraged research regarding the addition of CNCs to polymers and polymer composites. In fact, research has shown that inclusion of CNCs often leads to an improvement in the mechanical properties (e.g., tensile strength and modulus, impact strength, etc.) of the polymeric materials as well as fiber reinforced composites (FRCs) [40-42].

Previous work in our group showed CNCs to significantly increase the mechanical properties of both polymers and GFRPs. The effect of both CNCs and functionalized CNCs was investigated. The work by Asadi *et al.* showed that the addition of 1 wt% CNC in the epoxy matrix of SMC E-glass GFRPs resulted in an increase of 15% in elastic modulus, 11% in flexural modulus and 14% in flexural strength [43]. While the work completed by Haque *et al.* showed that spray coating E-glass fibers with a 1 wt% CNC solution resulted in 37% improvement in interfacial shear strength when compared to uncoated fibers [28]. Lastly, work by DiLoreto *et al.* shed some light on the effect of CNCs on unsaturated polyester resin and investigated the effect of CNC surface chemistry. The work demonstrated that the addition of 1 wt% CNC resulted in the flexural modulus increasing by 53% and the tensile modulus increasing by 22%. Additionally, the glassy modulus of the samples when 1 wt% of methyl(triphenyl) phosphonium-functionalized CNC or maleic acid-functionalized CNC was added to the resin increased by 61% and 66%, respectively [29].

1.2 Sheet Molding Compounds (SMC) Technology

1.2.1 General SMC Background

Sheet Molding Compounds (SMC) are fiber-reinforced semifinished materials. SMC materials are generally made of a thermoset matrix and glass fibers at a content of 10-65 vol% [13]. The SMC technology is widely used and favored for its high-volume production rate [44]. The general SMC process is presented in the flow chart in Figure 1-3 [45], and a more detailed description of the process is included in Chapter 2. Table 1-3 lists the components of a typical SMC formulation alongside their functions [46].

Figure 1-3: A flowchart describing the process of making SMC composites [45].

SMC materials are uncured composite sheets that are about 2-3 mm in thickness, and once prepared, they undergo a maturations process, usually a few days at ambient conditions or specific temperature and humidity depending on the formulation. These sheets are easily cut into the desired shape and weight for compression molding following their maturation period. There are multiple types of SMC distinguished by the orientation of the reinforcement material. SMC-R is made with randomly oriented short fibers. SMC-C uses continuous unidirectional fibers. SMC-CR uses continuous unidirectional fibers as well as randomly oriented short fibers. Lastly, XMC is made with a mixture of both randomly oriented short fibers as well as continuous fibers arranged in an X pattern. Figure 1-4 below shows a schematic of the different SMC products. The typical mechanical properties of a E-glass/polyester SMC composite are included in Table 1-4.

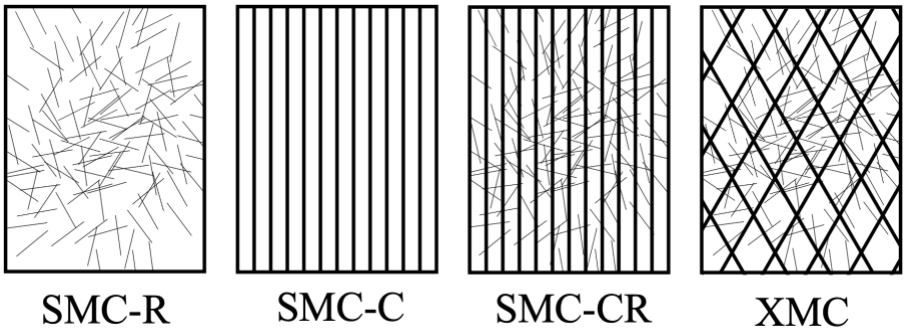

Figure 1-4: A schematic showing different SMC products [47].

Table 1-3: Components of a typical SMC material [46].

Component	Function	Weight %
Chopped glass fibers	Reinforcement	30.00
Unsaturated polyester resin	Base resin	10.50
Calcium carbonate	Filler	40.70
Styrene monomer	Co-monomer	13.40
Polyvinyl acetate	Low shrink additive	3.45
Magnesium oxide	Thickener	0.70
Zinc stearate	Mold release	1.00
t-Butyl peroxybenzoate	Catalyst	0.25
Hydroquinone	Inhibitor	Trace amount

Table 1-4: Typical properties of SMC (Polyester resin, $CaCO_3$ filler, and 25 wt% E-glass fibers) [13].

Density	1.85 g/cm3
Tensile modulus	10 GPa
Flexural modulus	10 GPa
Tensile strength	75 MPa
Flexural strength	170 MPa
Izod impact	800 J/m

1.2.2 Compression Molding

Once the SMC material is sufficiently matured, the sheets are cut, and a number of plies is placed in a pre-heated mold for compression molding. The mold is preheated to a temperature that would activate the catalyst to allow the composite to properly cure. These sheets, which are referred to as a charge, generally cover 30% to 90% of the mold area. As the material undergoes compression, flow is induced within the mold, and the mold cavity gets filled with the composite. Figure 1-5 shows a schematic of a typical compression molding process [13] [46].

Compression molding is advantageous for high-volume production rate, low-cost components, and the potential for high surface quality. Drawbacks of compression molding include the high capital investment required for setting up the equipment and machinery required for the process. Additionally, compression molding might introduce a variety of internal and external defects. Internal defects include blisters, high void content, weld lines and warpage. These defects can generally be mitigated through the

proper selection and handling of materials and equipment. External defects are associated with poor surface finish. Moreover, SMC technology and compression molding is not well suited for small scale runs and prototyping. [44, 48, 49].

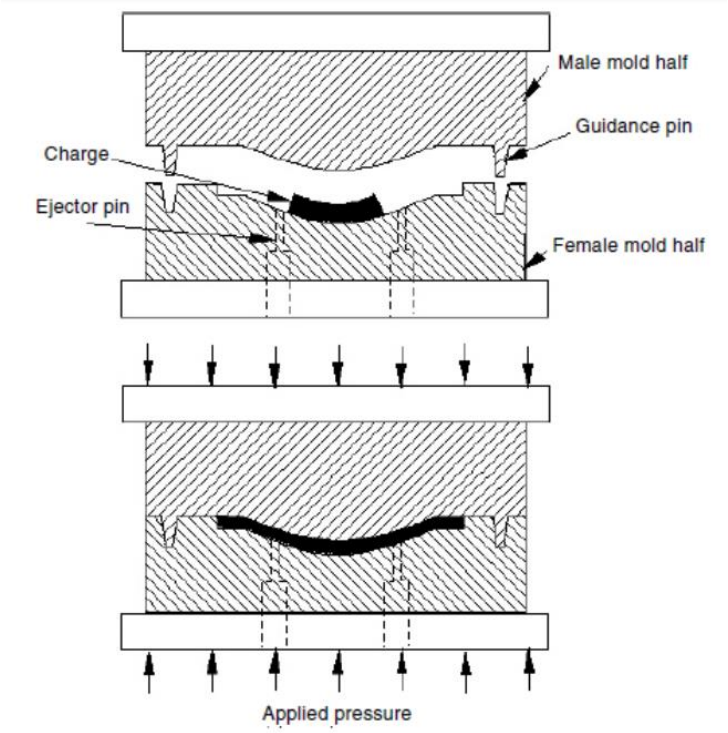

Figure 1-5: A schematic of a typical compression molding process [46].

1.3 Goal and Objectives

This work is concerned with investigating the potential of S2-glass fiber polyester composites by determining the effect of the sizing and the effect of adding CNCs into the polyester on the mechanical properties of the resulting composites. Specifically, it focuses on three different glass fiber sizing agents designed to produce high strength SMC composites. The question considered was regarding the possibility of improving flexural and tensile properties without compromising in impact properties by fine tuning

the sizing chemistry. Three different sizing agents were prepared and applied to the S2-glass rovings by AGY, a company that designs, develops, and manufactures glass fibers for different high demand industries, including automotive, aerospace and defense industries.

The three sizing agents were compared by characterizing the S2 glass fiber composites manufactured using an SMC pilot line. The sizing agent that resulted in the most optimal mechanical properties was then used for the second part of the project, which focused on investigating the effect of CNCs on S2-glass fiber composites. E-glass composites were also manufactured and tested as a reference. Composites with different concentrations of CNCs were manufactured using both E-glass and S2-glass. These composites were characterized in terms of tensile, flexural and impact properties. Dynamic mechanical analysis (DMA) was also utilized to compare the different composites. Additional characterization techniques, such as water displacement to determine the density of the composites and microscopy to study the composites' microstructure were also conducted.

The motivation for this work is twofold. First, it is commonly stated that glass fiber composites are not strong enough to be utilized in structural applications. This work seeks to ascertain whether glass fibers can possess suitable properties that deem them ideal for structural applications [50]. The second motivation is lightweighting. If stronger glass fibers are established, then their content in composites can be safely reduced, and since fibers are the heaviest component of composites, the overall density of the composite would decrease. This lightweighting would result in increased fuel efficiency and a more environmentally friendly design. This work seeks to accomplish this goal by

pursuing the research plan outlined in Table 1-5. The naming convention utilized throughout the project was as follows, (CNC PHR) (Glass Fiber Type) (Glass Fiber Sizing if applicable). Composites investigated in part 1 are, 0S2S, 0S2P, and 0S2R; while in part 2, they are, 0E, 2.5E, 0S2P, 2.5S2P, and 5S2P.

Table 1-5: Overview of the research plan.

Project Part	Parameters Investigated	Parameters range	Additional Characterization
Part 1	S2 Glass Fiber Sizing	**S2-S** **S2-P** **S2-R**	Visual inspection of morphology of sizing films (SEM). Assessing T_g of sizing polymeric film former (DSC). Examining functional groups present on glass fiber surfaces (XPS).
Part 2	Glass Fiber Type	**S2-glass** **E-glass**	Examining functional groups present on glass fiber surfaces (XPS).
	CNC	**0 PHR** (0 wt%) **2.5 PHR** (2.21 wt%) **5 PHR** (4.33 wt%) *	Assessing the quality of CNC dispersion (SEM).

*: Only prepared for S2-glass.

CHAPTER 2. MATERIALS AND METHODS

2.1 Materials

2.1.1 Resin

The resin used throughout this project was an isophthalic polyester resin, Pultru® P706-101, which was provided courtesy of AOC, a global supplier of specialty resins. Additional styrene purchased from Sigma-Aldrich was added to the resin. The catalyst used in this formulation was tert-Butyl peroxybenzoate and was purchased from Acros Organics. Zinc stearate, which was added to resin as mold release agent, was also purchased from Acros Organics. The thickener dispersion used, Accumag®-9033, was obtained from Chromaflo Technologies, a global supplier of chemical dispersions. Table 2-1 lists the different components used in the resin as well as their respective amounts

Table 2-1: Resin formulation details used throughout the project.

Component	More Details	Supplier	Weight (PHR)
Resin	PulTru® P706-101	AOC	90
Styrene	S4972	Sigma-Aldrich	10
Catalyst	tert-Butyl peroxybenzoate	Acros Organics	1.5
Mold Release Agent	Zinc Stearate	Acros Organics	5.0
Thickener	Accumag®-9033 MgO 40%	Chromaflo Technologies	4.0

2.1.2 Reinforcement and Additives

Multiple glass fiber types were used throughout this project. In the first part of the study, S2 glass fiber rovings with different sizings (S2-S, S2-P and S2-R) were used, where S, R, and P refer to a generic name of the sizing as provided by AGY. All S2 glass rovings were provided courtesy of AGY. The second part of the study used S2-P and boron-free E-glass fibers (with the commercial name of Advantex® P204, provided by Owens Corning).

CNCs with the commercial name CelluForce NCC® NCV100-NASD90 were obtained through CelluForce. This is a spray dried powder with a reported powder particle size ranging from 1 µm to 50 µm. Individual CNC particles within the powder were reported to have a length of 116 nm. The moisture content in the powder has been reported to be less than 6.0% [51].

2.2 Manufacturing and Fabrication

2.2.1 Resin Preparation

The different resin components were added into a 4L stainless-steel vessel, according to Table 2-1, and mixed with an IKA Eurostar 40 motor with a Cowell high shear mixing blade. The mixing tools were selected for their ability to homogenize the resin rapidly. Mixing was done at 1,200 RPM until the mixture was homogeneous, which took about 10 minutes. Higher RPM setting was not used to avoid introducing bubbles into the resin paste. Once the mixture was homogeneous, a thickening agent was added and mixed for 5 minutes at 1,200 RPM. During work for Chapter 4, CNCs were slowly added into the resin paste prior to the addition of the thickener. CNCs were added slowly into the

mixing vortex to improve their dispersion in the resin, and mixing was continued until all CNCs were added and a homogeneous paste has formed. Following the addition of the thickener, the resin mixture was allowed to thicken until it reached the desired viscosity range of 8000-11000 centipoise in about 3 hours for CNC-free resin and about 2 hours for the resin mixes with CNC. The viscosity was regularly checked using a Brookfield DV-I Prime viscometer.

2.2.2 Fabrication of SMC

This project utilized a pilot line SMC obtained from Finn and Fram, shown in Figure 2-1, which is similar to industrial-scale SMC lines with the notable difference being the width of the sheets that are manufactured. Industrial-scale lines are usually 1 m or 1.5 m in width, while the Finn and Fram line used is around 0.3 m in width. The resin paste was prepared and left to thicken to the optimal level viscosity as recommended by the resin manufacturer. The resin was then poured into the two resin reservoirs in the SMC line. Figure 2-2 shows a schematic representation of a typical SMC line. The amount of resin in the final composite was controlled adjusting the doctor blades gap accordingly. A carrier film, which sets atop a motorized conveyor belt, pulled the resin under the doctor blades resulting in a uniform layer of resin. Chopped fibers then fell on top of the resin film, and a second resin film was deposited on top, forming a sandwich structure of resin-fibers-resin which then underwent the compaction zone of the SMC line. The compaction zone consists of a series of calendaring rolls and the applied pressure facilitates the wetting of the fibers by the resin.

The amount of fibers in the composite is adjusted by tuning the fiber cutting speed, the conveyor belt speed, or the number of rovings fed into the machine. After the

sheet came out of the compaction zone, it was collected, and conditioned by leaving it in ambient conditions for a week until the resin has reached the optimum viscosity range for compression molding. In general, maturation varies from a few days to a few weeks depending on the type of resin being used.

Figure 2-1: A picture of the Finn and Fram SMC line used in this work [45].

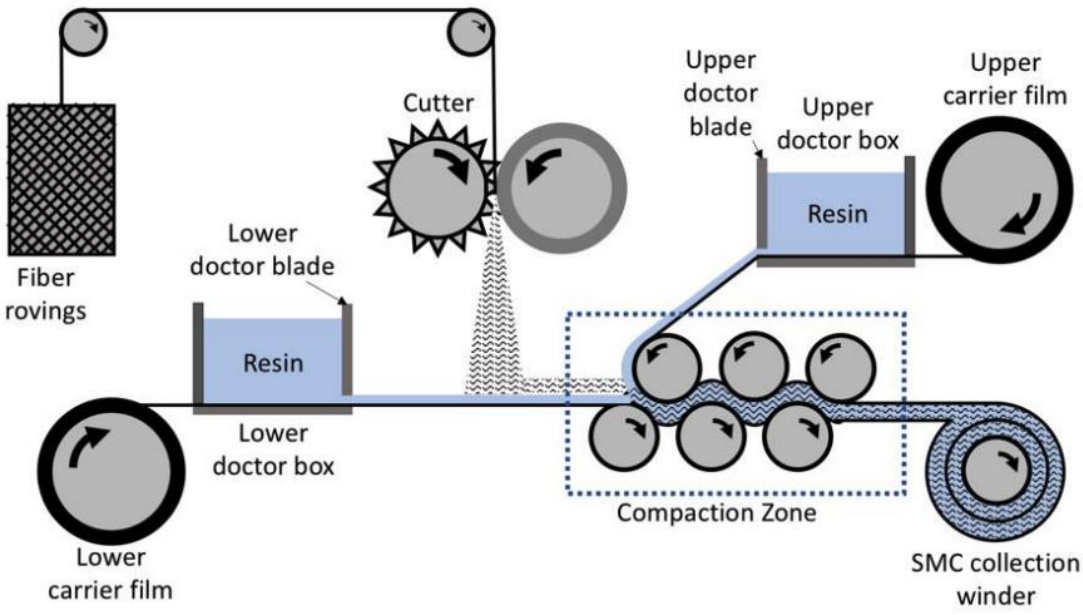

Figure 2-2: A simplified diagram of a typical SMC line.

2.2.3 Compression Molding

Following the fabrication of the SMC material and its maturation for a week, the sheet was cut into squares of around 150 x 150 mm^2, so that the outer edges of the SMC sheet was discarded. Four squares were placed in a pre-heated 279.4 x 279.4 mm^2 steel mold in an alternating manner to minimize any possible effect of the SMC line direction. The charge was trimmed to fill the mold cavity by using ~300g of the SMC material. The charge covered ~30% of the mold area, but once flow was induced, the mold cavity was filled. The mold was preheated to guarantee that the charge reached the desired cuing temperature in a short period. A 50-ton hydraulic hot-press (model V50-1818-2TMX, obtained from Wabash Metal Products Inc.) was used to mold the SMC charge. A pressure of 45 tons (~4.3 MPa), and a temperature of 150 °C were applied for 3 minutes.

2.2.4 Testing Coupons Preparation

Testing coupons were cut from the plates with the required geometry for each test using an OMAX- ProtoMAX water jet. Prior to cutting, the plates were stored at ambient conditions for at least 48 hours, and after cutting, the coupons were promptly dried and stored in ambient conditions in a desiccator to fully dry. In part 1, coupons were prepared with a cut quality of 3, and a machinability setting of 712.22 which corresponded to "Fiberglass Reinforced Vinylester Polymer". For part 2, the cut quality was increased to 5 for improved uniformity of testing coupons.

2.3 Characterization Techniques

2.3.1 Microscopy

A Phenom XL G2 SEM was used to examine the sizing layer on the fibers as well as to assess CNC dispersion for samples in part 2. Dispersion was assessed by attempting to locate any CNC agglomeration within the different composites. To limit surface charging effects, samples were Au/Pd sputter coated for 30 s at 0.1 mA using a Cressington 108 sputter coater. The SEM was used at an accelerating voltage of 15 kV.

2.3.2 Mechanical Testing

At least ten samples were tested for each test. Tensile and flexural properties were determined at ambient conditions using an Instron Universal test machine equipped with a 133kN (30,000 pound) load frame. The load frame was used in conjunction with a 45kN (10,000 pound) load cell, which is calibrated annually according to ASTM E4 [52].

During tensile testing, a clip-on extensometer (model 3542-025M-010, obtained from Epsilon Technology Corp.) with a gauge length of 25.4 mm was utilized. Coupons type I according to ASTM D638 [53] were prepared by waterjetting. The extensometer used is calibrated annually according to ASTM E83 [54]. The test was done at a displacement rate of 5 mm/min with an initial nominal strain rate of 0.05 mm/(mm·min).

Flexural properties were determined by employing the 3-point bending mode at a span-to-thickness ratio of 16 to 1 and a strain rate of 0.01 mm/(mm·min) corresponding to a crosshead displacement rate of 1.0 mm/min. The test coupons had the dimensions of 127 x 12.7 mm^2 according to ASTM D790 [55].

Both notched and unnotched coupons were tested under impact and the energy absorbed was reported. For part 1, testing was done with an Instron model SI-1C3 Pendulum Impact Tester of 300 ft-lb (406.7 J) capacity with a span of 40 mm. For each composite, 10 notched and 10 unnotched coupons were tested. The unnotched coupons had the dimensions of 62 x 12.75 mm^2 according to ASTM D4812 [56], and they had nominal thickness of 2.5 mm. The dimensions of the notched coupons in part 1 were 95 x 12.3 mm^2 and a nominal thickness of 2.5 mm. Dimensions were slightly different than what's specified by ASTM D6110 [57] in order to better suit the testing apparatus. The notch angle and radius were 45° and 0.25 mm, respectively as dictated by the testing standard.

For part 2, the pendulum energy was adjusted from 406.7J down to 169.5J by changing the latch position to improve testing accuracy. For each composite, 16 notched and 15 unnotched coupons were tested. The dimensions of the unnotched coupons were 64 x 13.4 x 2.5 mm^3. Notched coupons were further modified from the ASTM D6110 to

better suit the testing apparatus. The notch angle and radius were those dictated by the testing standard and were 45° and 0.25 mm, respectively. However, the dimensions of the notched coupons were 64 x 10.3 x 2.5 mm^3. Notches were made using the water jet.

Most samples didn't break completely. Unnotched samples experienced hinge breaks, while notched Charpy samples experienced partial breaks. Only data from similar break events were accounted for. The impact strength was normalized by the cross-sectional area of the specimen and reported in J/cm^2.

2.3.3 Density Measurements

Density measurements were carried out for each composite through the testing of at least 10 coupons weighing at least 500mg. The water displacement testing was done in accordance with ASTM D792 [58]. Samples were weighed in air using a Kern ACS220-4 with a resolution of 0.1 mg and were weighed in water using a Mettler Toledo AG245 with a resolution of 0.1 mg.

2.3.4 Determination of Constituent Content

Coupons from the cured composites were tested for constituent content following ASTM D2584 [59] . Samples were ignited within a Lindberg/Blue-M box furnace that was continuously operated at 635 °C to determine the weight of the non-volatile material within the composite. The weight of the combustible portion of the composite was determined as the difference between the coupon weight before and after ignition. The matrix weight was determined as 95 wt% of the combustible portion to account for the 5 wt% mold release agent within the resin. The noncombustible thickening agent was

estimated as 4 wt% based on the resin formulation. The glass fiber weight was calculated using Eq. (1), while the wt% of fibers was determined using Eq. (2).

$$net\ weight\ of\ glass\ fibers\ (g) = total\ nonvolatile\ material\ (g) - thickening\ agent\ (g) \quad (1)$$

$$glass\ fibers\ weight\ (\%) = \frac{100\ \times\ net\ weight\ of\ glass\ fibers\ (g)}{net\ weight\ of\ coupons\ prior\ to\ loss\ on\ ignition\ (g)} \quad (2)$$

2.3.5 Viscoelastic Properties

The viscoelastic properties were determined using a TA Instruments Q800 DMA according to ASTM D4065 [60] with the following conditions: oscillation of 1 Hz in 3-point bending mode with a span length of 50 mm and a strain of 0.1%; from 30 °C to 200 °C at a rate of 5°C/min. Samples had the dimensions 63 x 12.2 x 2.5 mm^3. 10 samples were tested for each composite in part 1, while 15 samples were tested for each composite in part 2. The relative size of the tan δ peaks was used to assess the material's ability to absorb impact energy.

Glassy modulus is reported as the storage modulus at 60 °C while the rubbery modulus as the storage modulus at 160 °C. Tan δ peaks were compared in two ways. The area under the curve was obtained by integration from 50 degrees below the temperature of tan δ peak to 50 degrees above (i.e. $T_{\tan \delta\ maximum} - 50$ °C, $T_{\tan \delta\ maximum} + 50$ °C). Lastly, literature suggests that broadening of tan δ peaks indicates improved fracture toughness and samples that are less prone to crack propagation and brittle failure, therefore, data for the full width half max (FWHM) of the tan δ peaks was reported [61].

2.3.6 Thermal Transitions

Differential scanning calorimetry (DSC) was carried on using a TA Instruments Discovery DSC to determine the T_g and to note any other thermal transitions associated with the different sizing formulations in part 1. Samples had a mass of ~10 mg and the tests were done from 30 °C to 200 °C at a rate of 10 °C/min. Three samples were characterized for each of the three uniquely sized S2 GF samples.

2.3.7 Glass Fiber Surface Analysis

The surface chemistries of the glass fibers were examined using Electron Spectroscopy for Chemical Analysis (ESCA), also known as X-Ray Photoelectron Spectroscopy (XPS). Characterization was conducted using a Thermo K-alpha XPS with an Aluminum K Alpha source gun. Samples were analyzed using a general survey scan with an energy step of 1.00 eV as well as specific element scans with an energy step of 0.1 eV. Elemental scans were done to better understand the bonding these elements were involved in, and it was done for multiple elements including Carbon, Oxygen, Silicon, and Aluminum. Three samples were characterized for each of the three uniquely sized S2 GF samples.

CHAPTER 3. UNDERSTANDING THE EFFECT OF S2 GLASS FIBERS SIZING ON THE MECHANICAL PROPERTIES OF S2 GLASS FIBER/POLYESTER COMPOSITES

3.1 Morphology of S2 GF Sizing

The three different sizing formulations were compared by examining the morphology of the sizing films. Sizing formulations S, P and R all had the same coupling agent, which provided polyester and vinyl ester compatibility, as well as the same additive package, which served as antistatic and lubricant. The basic difference among the three S2 glass fibers proprietary sizing was in the film former component of the sizing. SEM images of the three different S2 fibers are included in Figure 3-1.

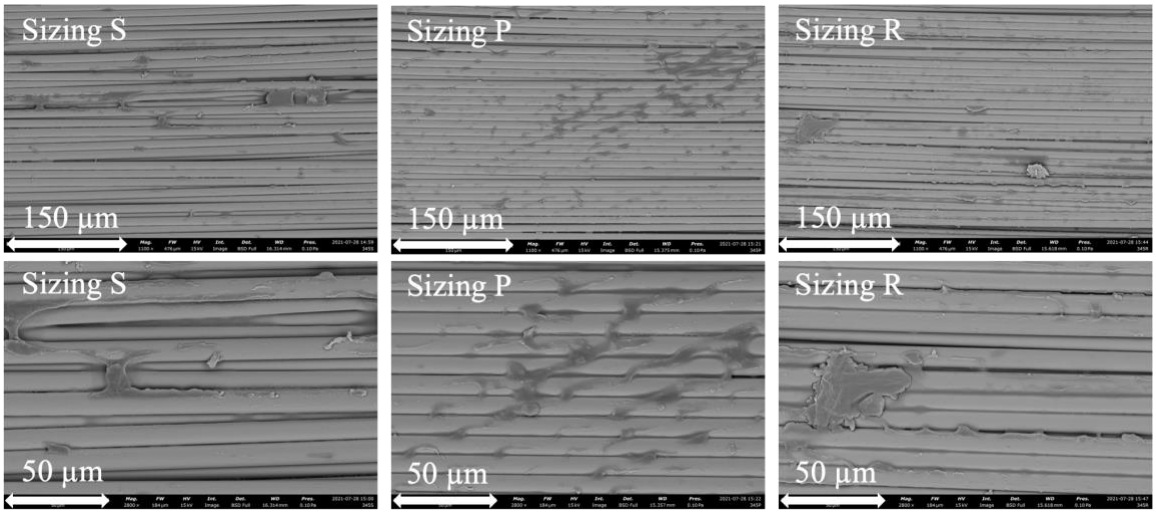

Figure 3-1: SEM Images of S2 glass fibers with the three different sizing formulations.

Examination of these images shows some of the qualitative differences between the different sizing films. Sizing P appears to be the most conforming to the fibers' surface. This is highly contrasted with sizing R, which possesses more defined edges. Sizing S is between sizing P and sizing R in conformability to the surface of the fibers. Increased conformability of the sizing film can be an indication of increased interfacial area which in turn results in improved interfacial strength.

3.2 Density, Glass and Void Content

The densities of the three different S2 GF/polyester SMC composites were measured via water displacement, and the loss on ignition method was utilized to obtain the GF wt% in the various composites investigated. Table 3-1 lists the experimental density from water displacement, the theoretical density, the void content obtained from the two previously mentioned densities in conjunction with Eq. (3), which is provided in ASTM D2734 [62], and the experimental GF wt% as obtained from loss on ignition tests.

$$Voids\ (vol\%) = 100 \times \frac{\rho_{theoretical} - \rho_{experimental}}{\rho_{theoretical}} \tag{3}$$

Table 3-1: Experimental and theoretical density, void, and GF content of the S2-GF/ polyester SMC composites as a function of the CNC content.

ID	$\rho_{experimental}$ *(g/cc)*	$\rho_{theoretical}$ *(g/cc)*	*GF (Wt%)*	*GF (Vol%)*	*Voids (Vol%)*
0S2S	1.53 ±0.03	1.54 ±0.03	38.6% ±3.4%	23.9% ±2.5%	0.89% ±0.52%
0S2P	1.55 ±0.02	1.57 ±0.02	41.8% ±2.2%	26.3% ±1.7%	1.08% ±0.27%
0S2R	1.59 ±0.05	1.61 ±0.04	45.5% ±3.7%	29.4% ±3.2%	1.15% ±0.66%

3.3 Mechanical Properties (Tensile, Flexural, and Impact)

Results from tensile and flexural testing were reported in relative terms to comply with AGY's corporate practices. Composites made with sizing R were set to be the baseline as that composite consistently performed the lowest in mechanical testing. Tensile and flexural properties are shown in Figure 3-2, and Figure 3-3, respectively. Impact strength results for both notched and unnotched coupons are included in Figure 3-4. For Figure 3-4 and subsequent box plots, the average is shown as a line horizontally crossing the box. The bottom whisker represents the lower extreme value, the bottom edge of the box represents the lower quartile, the top edge of the box represents the upper quartile, and the top whisker represents the upper extreme value.

Examining the results from the tensile and flexural tests, we see that 0S2R composites performed statistically lower in both tensile and flexural strength than 0S2S and 0S2P. Tensile modulus saw the highest increase for the 0S2S composites. Tensile strength of both 0S2S and 0S2P saw a notable increase compared to 0S2R. Flexural modulus didn't see any significant changes, while both 0S2S and 0S2P saw an increase in flexural strength, with 0S2P seeing a slightly bigger increase. In general, the tensile strength and modulus for composites with short randomly oriented fibers depend on the matrix stiffness and volume fraction, and the fibers stiffness and volume fraction, and on fiber dimensions [63]. All three composites were prepared using S2 GF and polyester resin, and the constituent volume fractions were consistent; therefore, it was expected that the composites would exhibit similar tensile modulus values. However, literature also suggests that tensile behaviour is dependent on the interfacial adhesion [64]. Analysis on tensile behaviour also applies to the flexural properties, since a material that is

undergoing flexural testing is undergoing both compressive and tensile forces. Since all other factors are identical, the differences in tensile and flexural strength and modulus were attributed to the different coating morphologies. Sizing R, which was described to have the least conforming sizing film and therefore the least amount of interfacial adhesion, exhibited the lowest values for strength and modulus, thus reinforcing the importance of sizing film conformability.

Impact testing shows that all the three different composites performed within range of each other, and that there was no GF sizing that resulted in statistically improved impact strength. However, it was noted that no statistically significant decrease in impact strength was coupled with the increases observed in tensile strength and flexural strength seen with 0S2S and 0S2P, which was generally a concern as increase in tensile strength is often coupled with decrease in impact strength. The energy absorbed by a polymer composite during impact can be better understood by understanding the impact energy absorbed due to fiber breakage, and the impact energy absorbed due to fiber pull-out. While there are other impact energy terms, their contributions are considered negligible as the behaviour of the material is largely dictated by the two previously mentioned impact energy terms [65]. The energy absorbed due to fiber breakage is dependent on fiber volume fraction, the fiber tensile strength and modulus, and test span length [66], while the energy absorbed due to fiber pull-out is dependent on the interfacial shear strength, fiber tensile strength, and fiber dimensions [67]. The three composites investigated only differed in the morphology of the sizing film. Therefore, the similar impact strength behaviour of the composites was expected.

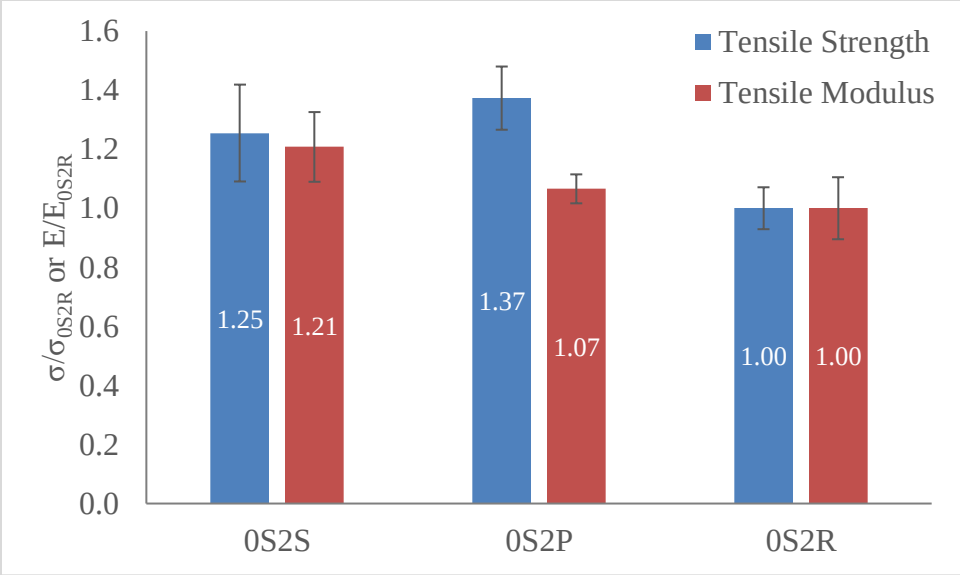

Figure 3-2: Tensile strength and modulus of S2-GF/polyester SMC composites as a function of the S2-GF sizing. Results are normalized with respect to the strength and modulus of the 0S2R composite to comply with AGY's corporate practices.

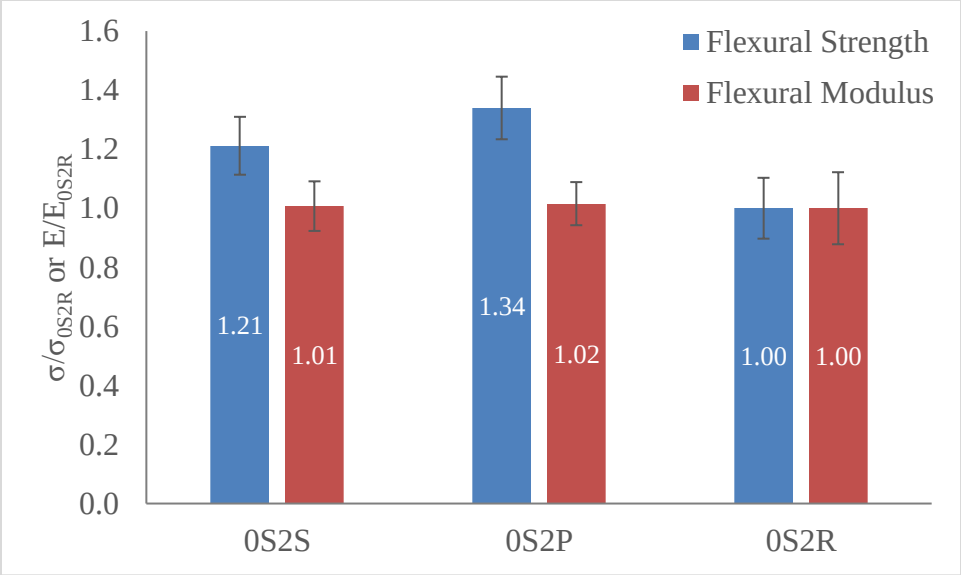

Figure 3-3: Flexural strength and modulus of S2-GF/polyester SMC composites as a function of the S2-GF sizing. Results are normalized with respect to the strength and modulus of the 0S2R composite to comply with AGY's corporate practices.

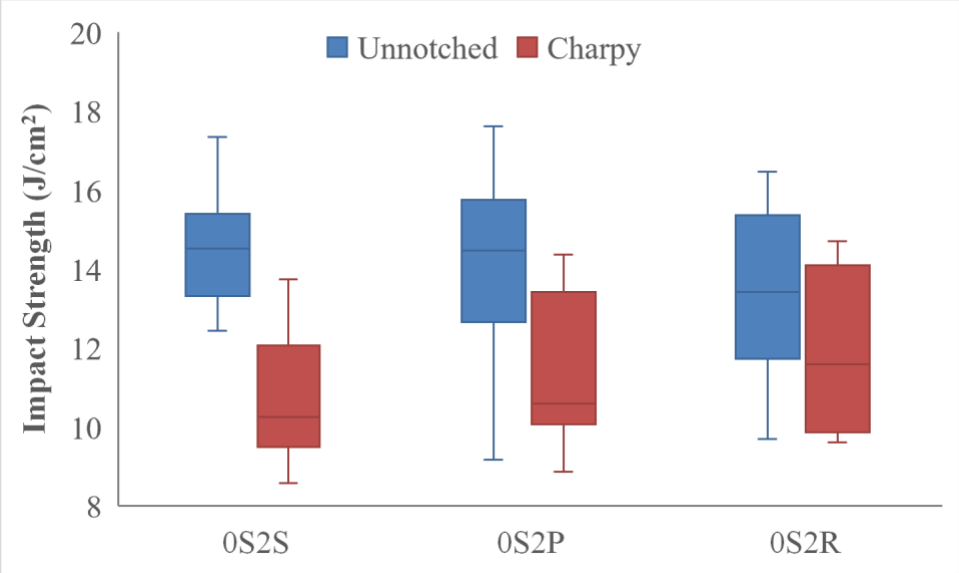

Figure 3-4: Impact strength for notched and unnotched S2-GF/polyester SMC composites as a function of the S2-GF sizing. Impact energy absorbed by the coupon was divided by the cross-section and reported in J/cm^2.

3.4 Thermomechanical Properties

The thermomechanical properties that were investigated were the glassy and rubbery moduli, and tan δ peak and they are shown in Figure 3-5 and Figure 3-6 respectively. As shown, there are no statistically significant differences among the composites made with the three differently sized S2 glass fibers. Values for dynamic modulus of composites depend on the level of stress/strain applied, the type of resin, the configuration of the laminates, fiber type, and other testing parameters [68]. The testing parameters including the level of strain applied, and all factors other than fiber type were identical among the three different composites. All three composites had S2 GF, but they differed in the sizing films. Therefore, thermomechanical properties were investigated to

determine the extent of effect that the coating morphology has on the properties of the composite. However, the change in coating morphology was evidently not significant enough to drastically influence the viscoelastic behavior of the composites. Glassy modulus is reported as the storage modulus at 60°C, while the rubbery modulus is reported as the storage modulus at 160°C.

Figure 3-5: Glassy and rubbery modulus values of the three different S2-GF/polyester SMC composites as a function of the S2 GF sizing. Obtained from 3-point-bending DMA tests.

Values of the area under the curve of the tan δ peak for the different composites are shown in Figure 3-6. All three composites had similar areas under the tan δ peak. The area under the curve was assessed as it's indicative of a material's toughness. As all three composites had similar impact strength, it was expected that the three composites would have comparable tan δ peak areas. Table 3-2 shows a collection of the viscoelastic properties of the different composites.

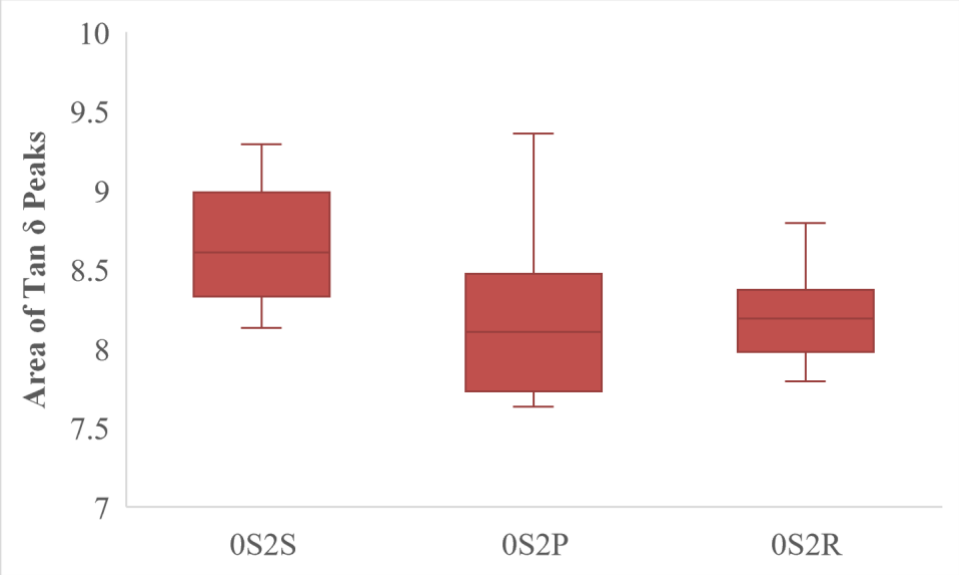

Figure 3-6: The area under the curve of the tan δ peak of the three different S2-GF/polyester SMC composites as a function of the S2 GF sizing. Integration was done from 50°C degrees below the tan δ peak maximum to 50°C degrees above the tan δ peak maximum. Obtained from 3-point-bending DMA tests.

A somewhat notable difference was the temperature at which Tan δ peak maximum was reached. Although within range of the other S2 GF sizing formulations, it was a point of interest, and therefore thermal transitions of the S2 glass fibers polymeric sizing film were investigated. Figure 3-7 below shows an overlay of DSC curves for the differently sized S2 glass fibers. No thermal transitions were noted. This was attributed to the low amount of sizing material on the glass fibers, as sizing is generally added to be less than 2 wt% of the fibers [18], and this amount was not sufficient to indicate where the glass transition temperature of the polymeric film component of the sizing takes place.

Table 3-2: Viscoelastic properties of composites made with differently sized S2-GF obtained from 3-point-bending DMA tests.

ID	*Temperature at Tan δ Peak (°C)*	*Area of Tan δ Peaks*	*Tan δ Peak FWHM*	*Glassy Modulus (MPa)*	*Rubbery Modulus (MPa)*
0S2S	110 ±1.7	8.6 ±0.4	73.8 ±5.6	8145 ±1339	2732 ±558
0S2P	110 ±1.5	8.2 ±0.5	78.0 ±6.8	8182 ±884	2960 ±331
0S2R	114 ±1.6	8.2 ±0.3	79.6 ±4.7	9690 ±919	3614 ±419

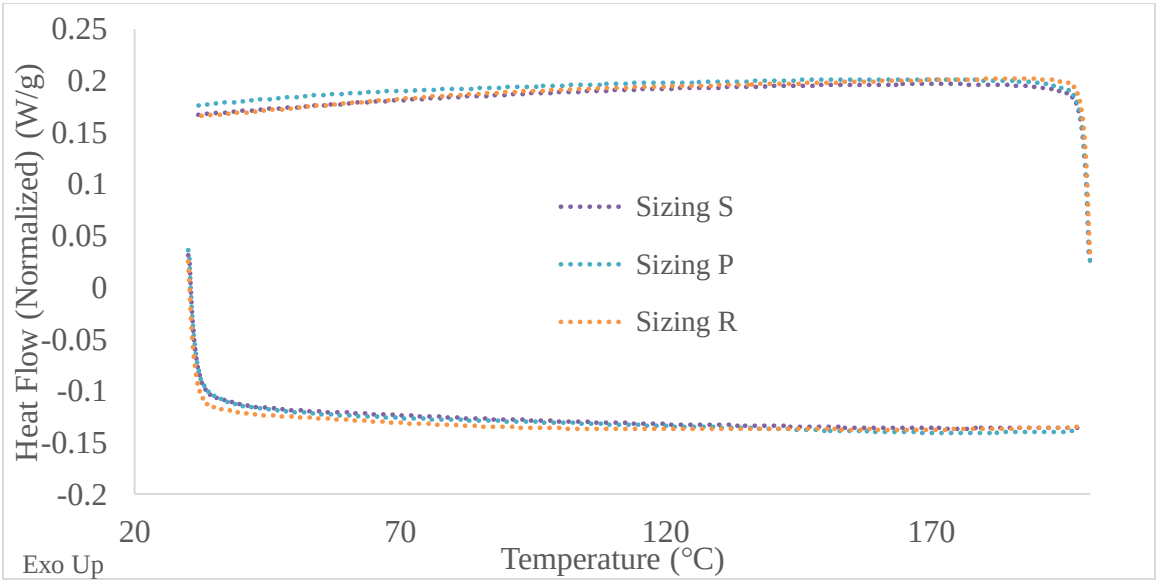

Figure 3-7: DSC curves of three S2-GF samples with different sizing formulations. Heating rate was 10 °C/min. T_g of polymeric film of the sizing was not noted.

3.5 Glass Fiber Surface Analysis

Surface chemistries of the glass fibers were investigated by utilizing XPS. C1s scans were of a particular note as they illustrate the nature of bonding carbon atoms are involved in, which was then further analyzed to ascertain information regarding functional groups within the sizing. Figure 3-7 shows an overlay of the C1s scans of the three different S2 GF sizing formulations, while Table 3-3 below shows the concentration of the different types of carbon bonding within the sample.

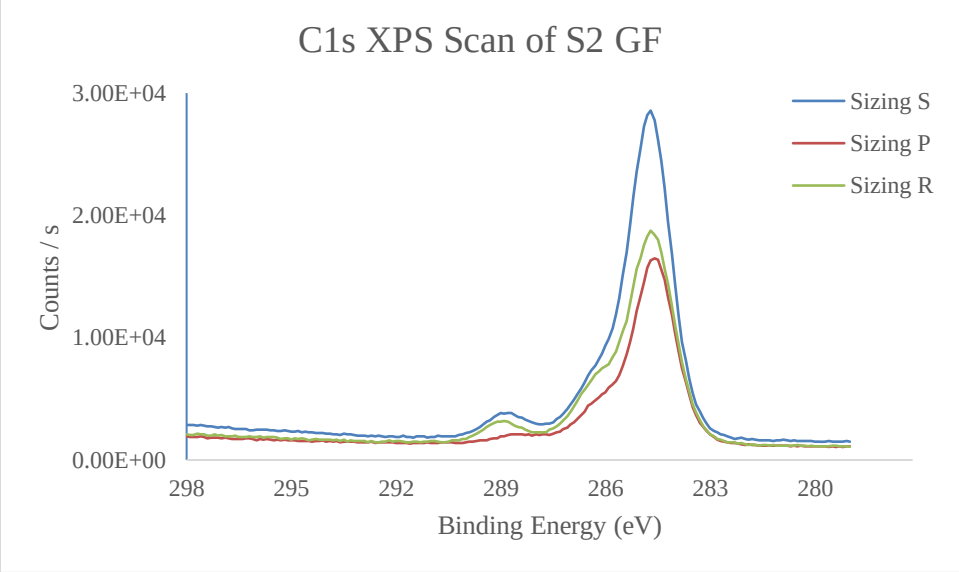

Figure 3-8: C1s XPS of S2-GFs with different sizing formulations.

Table 3-3: Numerical description of carbon bonding within the glass fiber sizing as obtained from XPS C1s spectra.

ID	*C-C Atomic%*	*C-O-C Atomic%*	*O-C=O Atomic%*
S	80.0 ±1.5	13.6 ±1.1	6.4 ±0.8
P	81.6 ±1.6	12.7 ±2.4	4.7 ±1.2
R	81.2 ±1.9	12.6 ±1.6	6.2 ±0.7

Examining Table 3-3, we see that sizing P had the least concentration of ester functional groups, and while the difference wasn't statistically significant, one might expect that because the matrix utilized was a polyester resin, sizing P might perform most poorly. However, these percentages don't indicate the absolute amounts, and a lower percentage might translate to a larger number of functional groups.

The sizing on glass fibers is typically on the order of 500nm, while XPS has an information depth of around 10nm [69]. In other words, detecting elements that are only present within the glass fibers themselves indicates a glass fiber surface that wasn't covered by the sizing film. Atomic analysis, namely for C, O, Si, and Al, was conducted on the different GF samples. Characterization results can be seen in Table 3-4 and Figure 3-9.

Table 3-4: Atomic% of C, O, Si, and Al for the different S2-GF samples. Obtained from XPS Spectra.

ID	*C1s Atomic%*	*O1s Atomic%*	*Si2p Atomic%*	*Al2p Atomic%*
S	54.9 ±7.2	29.1 ±4.4	11.6 ±2.0	4.1 ±1.1
P	51.5 ±8.6	31.2 ±4.4	13.0 ±2.4	4.7 ±1.0
R	66.9 ±6.7	22.5 ±4.7	7.4 ±2.5	1.9 ±0.3

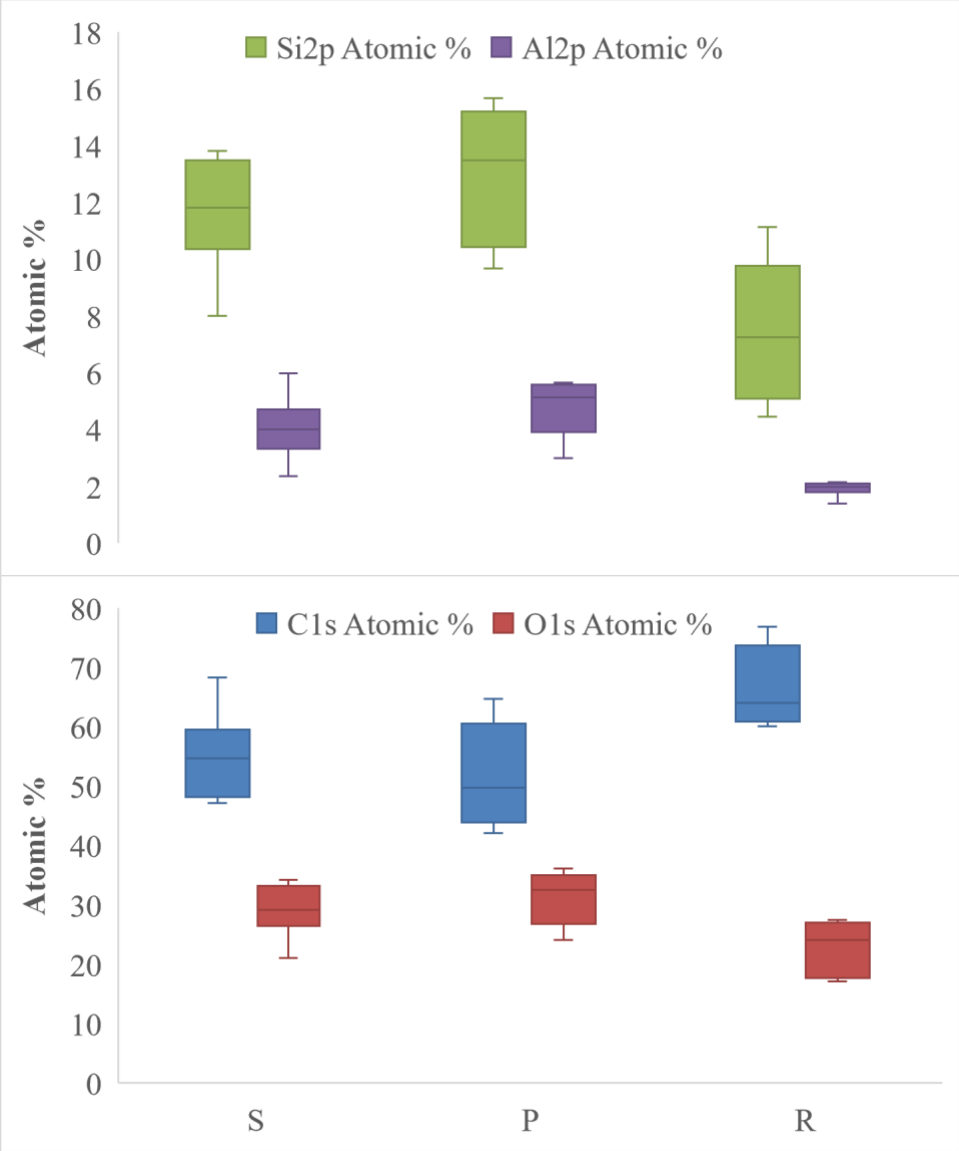

Figure 3-9: Atomic% of C, O, Si, and Al for the different S2-GF samples as a function of sizing.

Table 3-4 reveals more interesting information as sizing S and sizing P, which performed better than sizing R mechanically, had the least amount of C1s atomic%. It's of note that the C1s atomic% column refers to the peak that corresponds to C-C single bond (corresponding to 284.8 eV). Therefore, sizing R had the least potential to have functional groups as more of its carbon atoms are engaged in single bonding with another

carbon atom. Additionally, the increased amount of oxygen in the sizing is indicative of the sizing potential to interact with the ester groups present in the matrix. Sizing R had the least amount of aluminium which suggests increased sizing coverage compared to the other two sizing formulations. The functional groups present in sizing R are less evident compared to the other formulations. Figure 3-10 showcases possible sizing qualities in terms of coverage, thickness, and density of accessible functional groups.

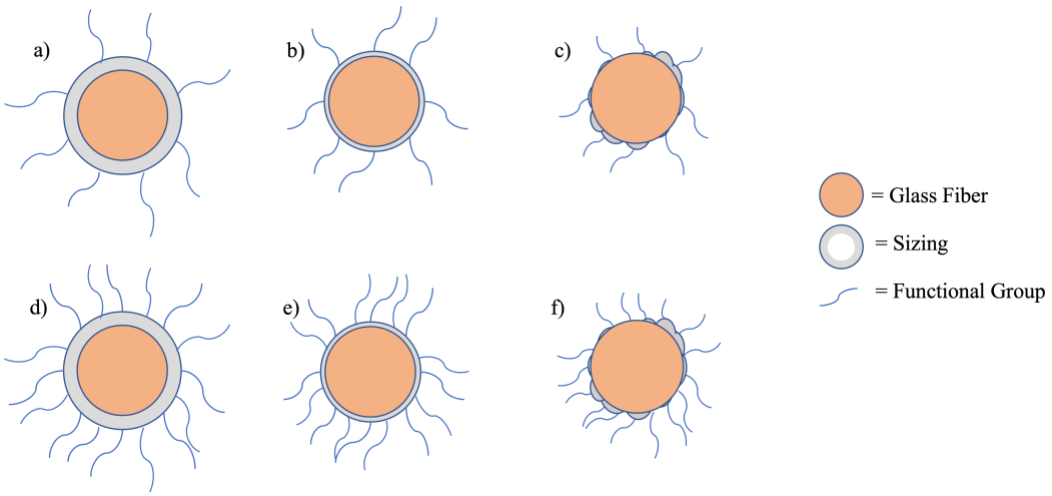

Figure 3-10: Possible sizing arrangements. a) thick uniform sizing with moderate functional group density. b) thin uniform sizing with moderate functional group density. c) erratic sizing with moderate functional group density. d) thick uniform sizing with high functional group density. e) thin uniform sizing with high functional group density. f) erratic sizing with high functional group density.

The generally improved tensile and flexural properties of 0S2P composites without a decrease in the impact properties coupled with surface chemistry that's more suitable for polyester resins indicate that sizing P was the most optimal sizing formulation. Also, sizing P had a noticeably more conforming sizing film. Therefore, the

second portion of this study, which is concerned with the effect of CNCs, utilized sizing formulation P for S2 GF.

CHAPTER 4. UNDERSTANDING THE EFFECT OF CELLULOSE NANOCRYSTALS ON THE MECHANICAL PROPERTIES OF S2 GLASS FIBER/POLYESTER COMPOSITES

4.1 Introduction

In addition to investigating the potential for enhancing the performance of S2-GF/polyester SMC composites by optimizing the fiber sizing, the possibility of enhancing the polyester resin by adding cellulose nanocrystals was also investigated. This study was motivated by prior results obtained by our group, a brief overview of which was provided in Chapter 1. The naming convention for samples in this chapter is as follows, (CNC PHR) (Glass Fiber Type) (Glass Fiber Sizing if applicable). Composites investigated in this chapter are, 0E, 2.5E, 0S2P, 2.5S2P, and 5S2P.

4.2 CNC Dispersion

This work incorporated CNCs into the matrix by mixing them in with the resin during the preparation of the paste that is used in the SMC line. It is expected that this method of adding the nanocellulose will not lead to homogeneous dispersion at the single particle level and formation of agglomerates will be unavoidable. However, it is the simplest and most expeditious and economical method and therefore most suitable for industrial applications. SEM was used to examine whether CNCs had agglomerated within the matrix. As shown in Figure 4-1, no noticeable CNC agglomeration form as the CNC content increases. Agglomerates as big as 5 microns can be seen in the images, but the agglomerate size did not change with CNC concentration, at least for the

concentrations investigated in this study. Additionally, the low number of voids and their relatively small size is in agreement with the low void content measured experimentally (presented in section 4.2).

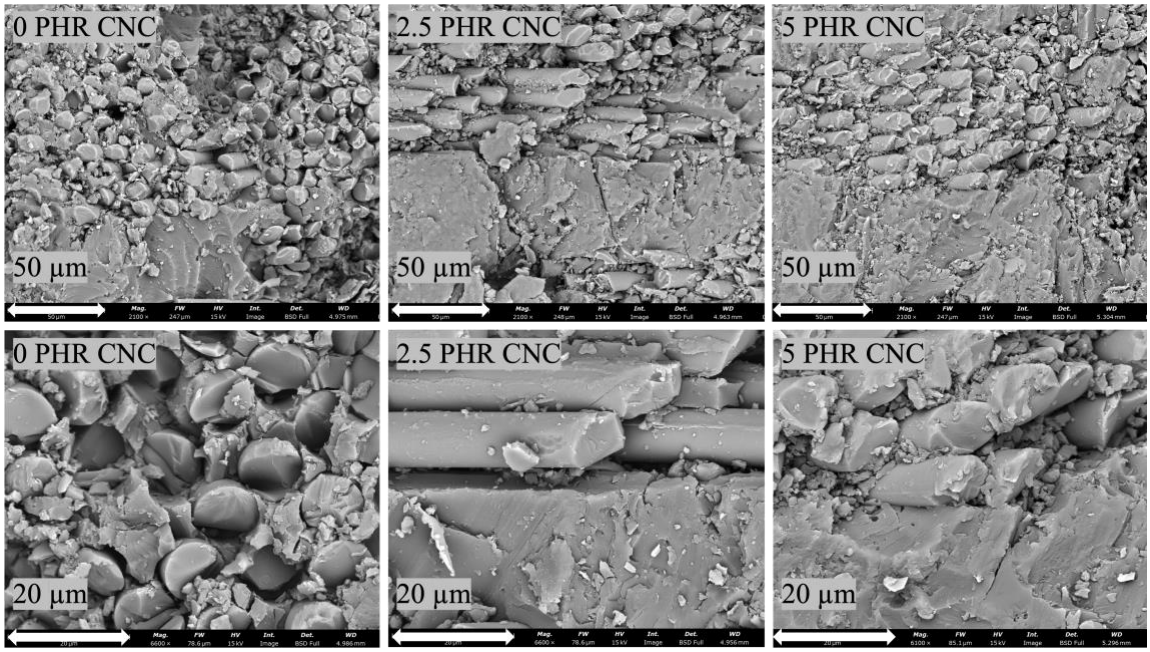

Figure 4-1: SEM images of S2P composites as a function of CNC content: 0 PHR (left), 2.5 PHR (center) and 5 PHR (right).

4.3 Density, Glass and Void Content

Table 4-1 shows the densities and constituent content of the S2 glass fiber CNC/polyester composites as a function of the CNC content. The details outlined in section 3.1.2 are also applicable for this section. The experimental densities, as measured via water displacement, range between 1.49-1.59 gg/cc, with 0S2P and 2.5S2P exhibiting the lowest values. This difference is reflected in the higher void content and lower GF vol% of those composites, however it is not statistically significant, and it can be

attributed to experimental error. It is noted that moving forward, results presented should be examined with the GF vol% in mind.

Table 4-1: Experimental and theoretical density, void and GF content of the E-GF and S2-GF/ polyester SMC composites as a function of the CNC content.

ID	$\rho_{experimental}$ *(g/cc)*	$\rho_{theoretical}$ *(g/cc)*	*GF Wt%*	*GF Vol%*	*Voids Vol%*
0E	1.58 ±0.01	1.59 ±0.01	41.8% ±1.4%	25.7% ±1.1%	0.48% ±0.22%
2.5E	1.59 ±0.02	1.61 ±0.03	42.1% ±2.6%	32.0% ±9.8%	1.35% ±0.70%
0S2P	1.53 ±0.02	1.56 ±0.02	39.1% ±2.0%	24.2% ±1.5%	2.02% ±0.20%
2.5S2P	1.49 ±0.02	1.52 ±0.02	34.2% ±1.9%	20.6% ±1.4%	1.74% ±0.29%
5S2P	1.57 ±0.03	1.59 ±0.03	42.0% ±2.8%	26.7% ±2.2%	1.48% ±0.27%

Density measurements and determination of the GF and void content is necessary to ensure the different composites are comparable and that differences in properties are a result of the addition of CNCs. Considering that the addition of CNCs in the resin matrix could increase the viscosity of the resin, which in turn may alter the resin flow and the wetting of the fibers and thus the properties of the composites, viscosity measurements, were conducted using a Brookfield DV-I Prime viscometer, for resin mixtures with 0 PHR, 2.5 PHR CNC and with 5 PHR CNC. The viscosity window that was targeted was suggested by the resin supplier and it was 8000-11000 cP. Within this optimal viscosity window, the resin is thin enough to properly wet the fibers, but not too thin that it squeezes out [13]. Resin mixture with 0 PHR reached the desired viscosity window in

around 3 hours. The viscosities of the 2.5 PHR and 5 PHR resin mixtures were expectedly higher, therefore they were allowed to thicken for around 2 hours. The two resin mixtures with CNC had similar viscosities.

4.4 Mechanical Properties (Tensile, Flexural, and Impact)

The mechanical properties, specifically the tensile and flexural properties and the impact strength, of the 5 different composites were determined. Tensile and flexural properties are reported in relative terms to comply with AGY's corporate practices. The baseline was set using composites made with E-glass and 0 PHR CNC (0E), as this composite consistently performed the lowest in mechanical testing. The tensile and flexural properties are given in Figure 4-2, and Figure 4-3, respectively. The impact strength for both notched and unnotched coupons is presented in Figure 4-4. Figure 4-4 is a box plot and directions regarding interpreting the plot were provided in section 3.3.

Examining the tensile and flexural data, we see that the addition of CNCs does not seem to increase modulus or strength in a statistically significant manner. This is a deviation from the expected result as theoretical models and previously cited work showed an increase in the modulus following the addition of CNCs. This might be an effect of suboptimal CNC dispersion within the matrix. Another possible reason for the deviation from what was expected might be the slightly variable glass and void content in the different composites which may offset any positive effect of the CNCs. Additionally, there is a large overlap of the standard deviations of the tensile and flexural properties of the different composites, therefore observed differences are not statistically significant.

One point of note was the tensile and flexural performance of composite 5S2P. Not only was this composite expected to outperform the other composites due to the

addition of CNCs, but 5S2P possessed marginally higher amount of GF, and had a lower void content than the other S2P composites. Testing was redone to ensure the repeatability of tensile and flexural tests, and the same pattern held true. It's suspected that CNC particles might have had some agglomeration which has been previously reported to decrease the strength of the composite [43].

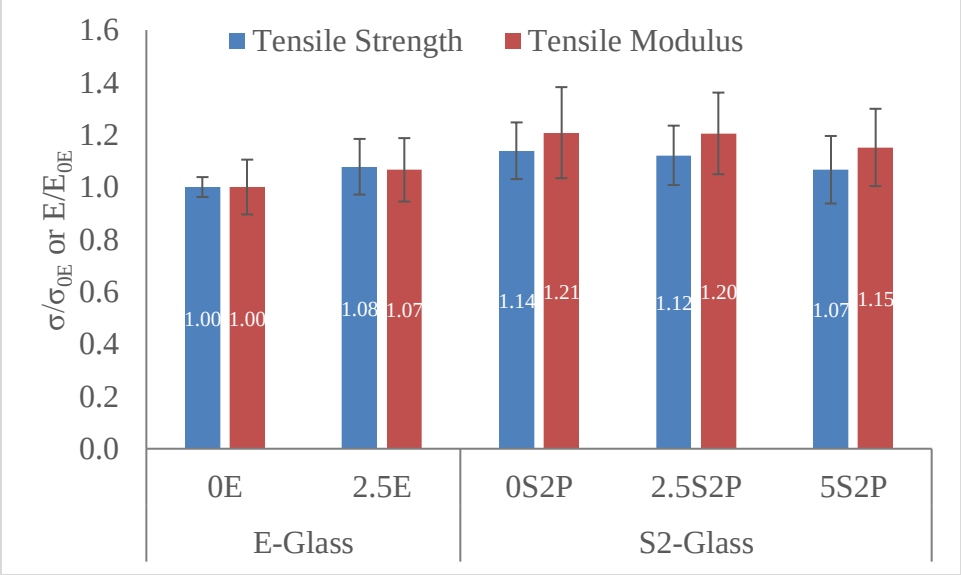

Figure 4-2: Tensile strength and modulus of E-GF/polyester and S2-GF/polyester SMC composites as a function of fiber type and CNC content. Results are normalized with respect to the strength and modulus of the 0E composite to comply with AGY's corporate practices.

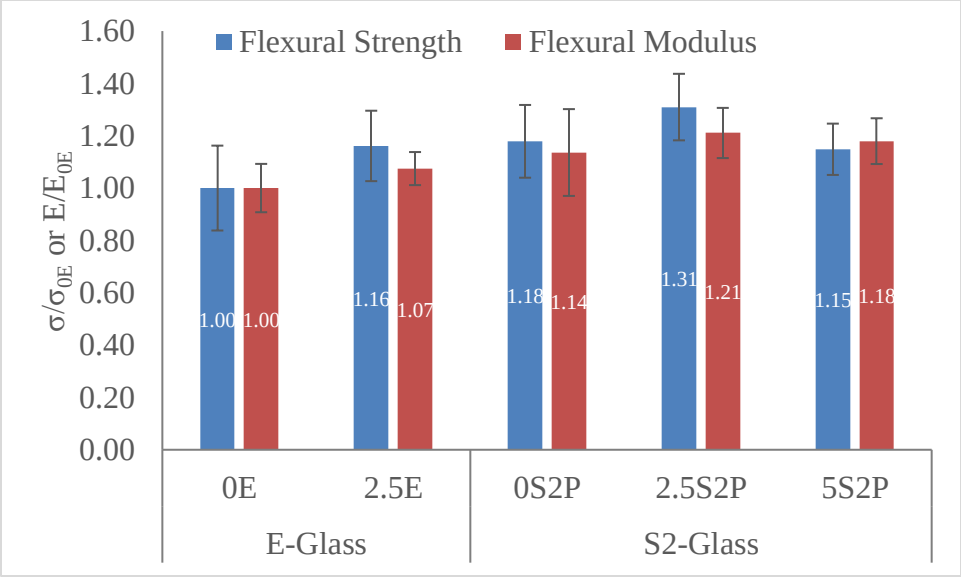

Figure 4-3: Flexural strength and modulus of E-GF/polyester and S2-GF/polyester SMC composites as a function of fiber type and CNC content. Results are normalized with respect to the strength and modulus of the 0E composite to comply with AGY's corporate practices.

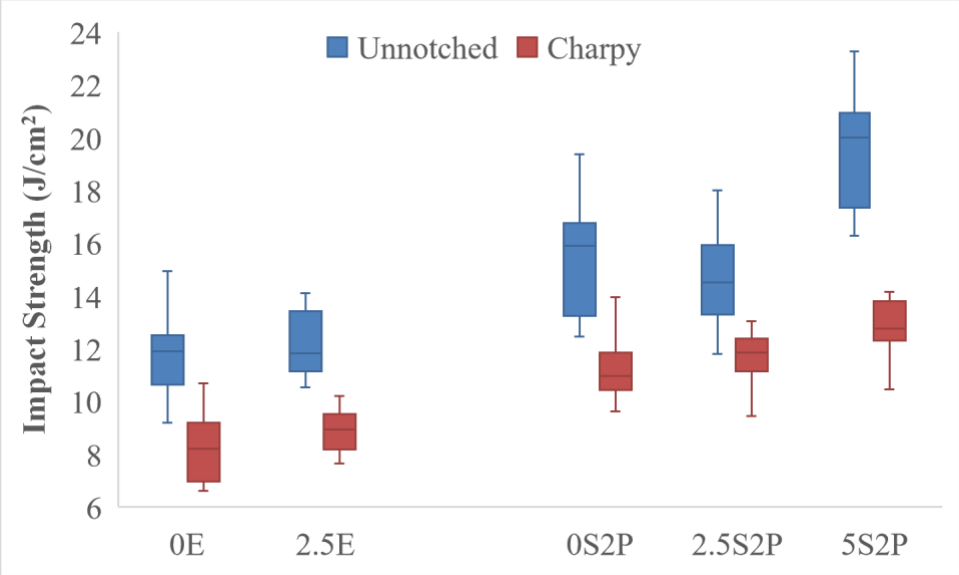

Figure 4-4: Impact strength for notched and unnotched E-GF/polyester and S2-GF/polyester SMC composites as a function of fiber type and CNC content. Impact energy absorbed by the coupon was divided by the cross-section and reported in J/cm^2.

Figure 4-4 provides more actionable insights as it suggests that the impact strength in case of both the S2 and E-glass is proportional to the CNCs content. Only composite 2.5S2P seems to lag behind the suggested trend, and this is attributed to the lower glass content in this composite. There is an overlap in the standard deviation among the different samples. That is, the various results fell within one standard deviation of the other composites of the same fiber type. However, it is observed that the average impact strength for both the notched and unnotched specimens increased with increasing CNC content.

Considering that these composites contain short fibers randomly distributed in plane, the Halpin-Tsai model, shown in Eq. (4) – Eq. (8) [70], was used to predict the

elastic modulus of these composites. In the case of composites containing CNCs, the modulus of the polyester matrix was first calculated using the Halpin-Tsai model and considering the CNC particles as the reinforcement. The Halpin-Tsai model assumes that fiber cross-section is circular, that fibers are arranged in a square array, that fibers are uniformly distributed throughout the matrix, that perfect bonding exists between the fibers and the matrix, and finally, that the matrix is free of voids. Eq. (4) and Eq. (5) were used to determine the uniaxial elastic modulus parallel to the fibers, and perpendicular to the fibers, respectively. l_f and d_f are the fiber/reinforcement length and diameter, respectively. v_f is the volume fraction of the fibers, and E_f and E_m are the elastic moduli of the reinforcement and the matrix, respectively [70] [71]. Eq. (8) was then used to estimate the elastic modulus of an FRP with randomly oriented fibers.

GF vol% used was kept constant and it was the average of the experimentally measured GF vol% of the different composites presented in Table 4-1, which was 25.8%. Figure 4-5 shows the different values of elastic modulus obtained using the Halpin-Tsai model. The data is reported in terms of E/E_{0E} to match with the tensile testing results presented earlier. l_f used was 25,400 µm (SMC parameter) and d_f for S2-glass was 11 µm, and 14.4 µm for E-glass. The elastic modulus used for S2-glass was E_f = 89.9 GPa. [11], and for E-glass, E_f = 80.0 GPa [72]. For CNC, l_f = 0.116 µm, d_f = 0.004 [51], and E_f =140 GPa [73]. The elastic modulus of matrix used was E_m = 3.03 GPa [74]. While it's expected that the Halpin-Tsai model overestimates the properties of the composite due to its idealistic assumptions, it does help outline the potential of CNCs in improving the elastic modulus by virtue of CNCs increasing the modulus of the matrix. It's noted that

this model does not account for any interactions between the CNCs and the matrix chains.

$$E_{11} = \frac{1 + 2\left(\frac{l_f}{d_f}\right)\eta_L v_f}{1 - \eta_L v_f} \tag{4}$$

$$E_{22} = \frac{1 + 2\eta_T v_f}{1 - \eta_T v_f} \tag{5}$$

$$\eta_L = \frac{\left(\frac{E_f}{E_m}\right) - 1}{\left(\frac{E_f}{E_m}\right) + 2\left(\frac{l_f}{d_f}\right)} \tag{6}$$

$$\eta_T = \frac{\left(\frac{E_f}{E_m}\right) - 1}{\left(\frac{E_f}{E_m}\right) + 2} \tag{7}$$

$$E_{random} = \frac{3}{8}E_{11} + \frac{5}{8}E_{22} \tag{8}$$

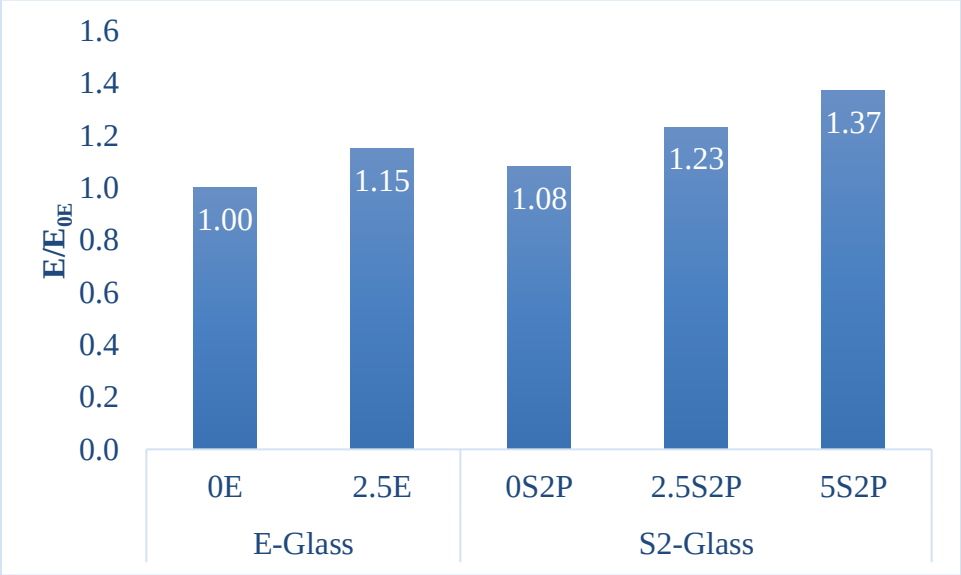

Figure 4-5: Predicted values of the elastic modulus of E-GF/polyester and S2-GF/polyester composites as a function of fiber type and CNC content. Results are normalized with respect to the modulus of the 0E composite. Obtained using the Halpin-Tsai and E_{random} equations.

4.5 Thermomechanical Properties

Figure 4-6 shows the glassy and rubbery moduli for the 5 different composites obtained from 3-point-bending DMA tests. Glassy modulus is reported as the storage modulus at 60°C, while the rubbery modulus is reported as the storage modulus at 160°C. 16 samples were tested for each composite, but the large overlap of the standard deviations of the modulus values indicates that the differences observed are not statistically significant.

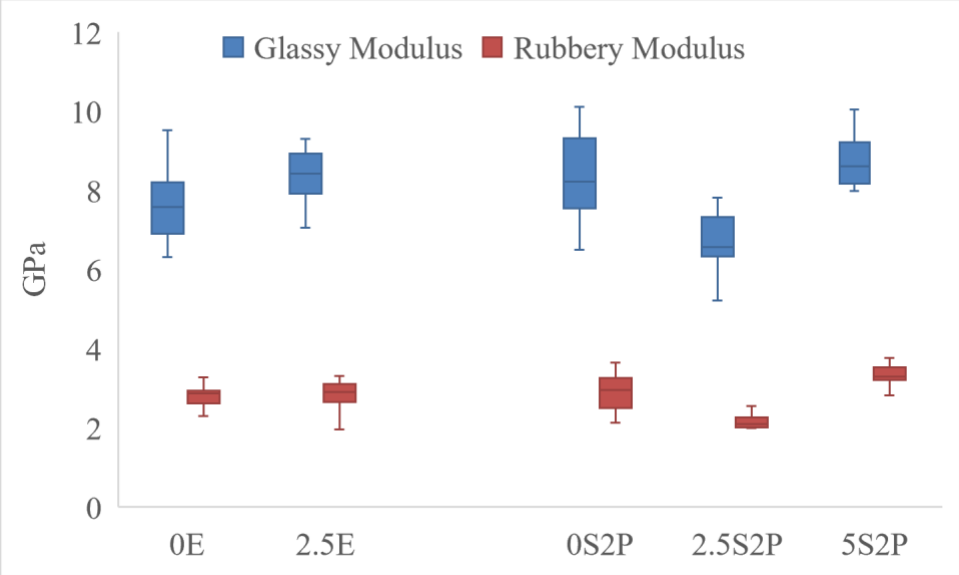

Figure 4-6: Glassy and rubbery modulus values of the 5 different E-GF/polyester and S2-GF/polyester SMC composites as a function of glass fiber type and CNC content. No clear trend observed.

Variation in GF vol% prevents meaningful comparisons of the moduli. However, if the data is normalized by the GF vol%, as in Eq. (9), a more meaningful plot emerges, which is given in Figure 4-7.

$$E_{Composite\ i,Normalized} = \frac{E_{Composite\ i,Measured} \times (GF\ vol\%)_{average}}{(GF\ vol\%)_{Composite\ i}} \quad (9)$$

The data in Figure 4-7 was normalized using Eq. (9) in conjunction with the GF vol% presented in Table 4-1 and the average GF vol% which was 25.8%. The figure suggests that the addition of CNCs decreases both rubbery and glassy moduli. However, the difference of both moduli among the different composites was not statistically significant. Examining Figure 4-8, we can see that the addition of CNCs has increased the

T_g (defined here as the peak of the tan δ) of the composites, with the difference between T_g of 0S2P and T_g of 5S2P being statistically significant. This is likely a result of the CNC particles restricting the mobility of the polymer matrix chains, therefore, shifting the glass transition temperature to higher temperatures. This is also an indication of the interactions between the matrix and the CNC additive. CNCs' restriction on matrix chain mobility has been observed by multiple researchers in the past [75-77]. Increase in T_g is also an indication of the improved thermal stability of the composites. Table 4-2 shows a tabulation of the various properties obtained from DMA. The area under the curve for the tan δ peaks of the different composite, which was interpreted to be an indication of a materials' resistance to impact fracture, did not correlate with the observed impact strength of the composites as it was expected that the area under the tan δ curve to correspond to the composite impact energy as suggested in literature [61]. However, values of the area under the curve for the different composites were within 1 standard deviation of results obtained for the other composites, therefore, the differences between the areas under the curve of tan δ were not statistically significant.

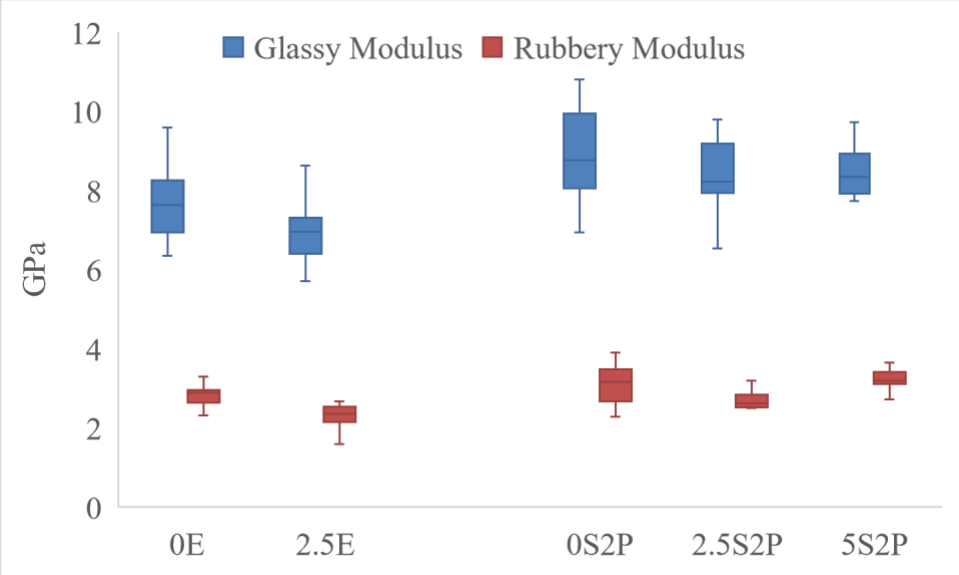

Figure 4-7: Normalized glassy and rubbery modulus values of the five different E-GF/polyester and S2-GF/polyester SMC composites as a function of glass fiber type and CNC content. Modulus decreased proportionally with the addition of CNCs without statistical significance.

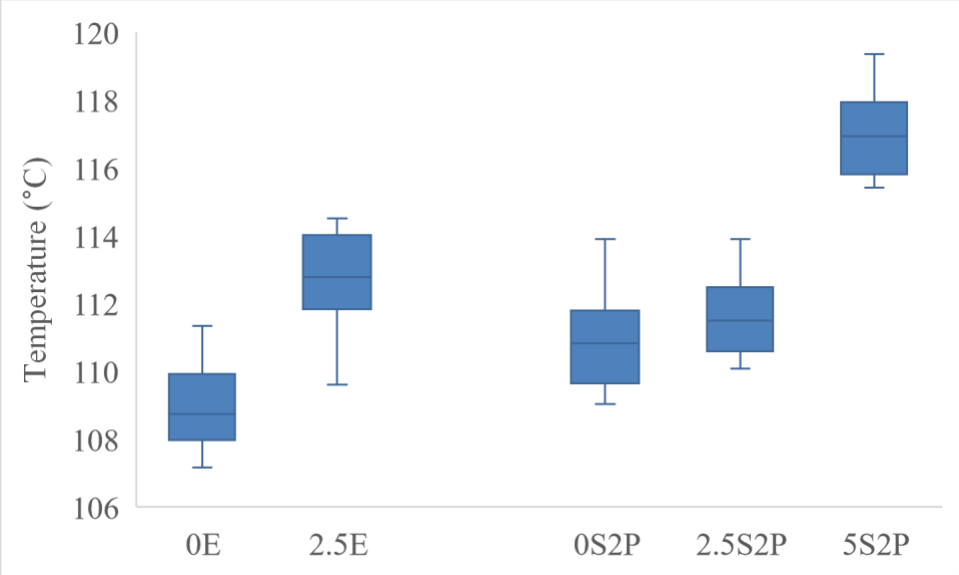

Figure 4-8: T_g, temperature at tan δ maximum, as obtained from 3-point-bending DMA tests of the five different E-GF/polyester and S2-GF/polyester SMC composites as a function of the glass fiber type and CNC content.

Table 4-2: Viscoelastic properties of the five different E-GF/polyester and S2-GF/polyester SMC composites as a function of the glass fiber type and CNC content. Obtained from DMA 3-point-bending DMA tests.

ID	*Temperature at Tan δ Peak (°C)*	*Area of Tan δ Peaks*	*Tan δ Peak FWHM*	*Glassy Modulus (MPa)*	*Rubbery Modulus (MPa)*
0E	109 ±1.3	8.0 ±0.6	77.0 ±5.6	7635 ±937	2811 ±265
2.5E	113 ±1.5	8.0 ±0.4	76.7 ±6.7	8405 ±632	2837 ±384
0S2P	111 ±1.4	8.3 ±0.3	76.9 ±2.9	8359 ±1047	2906 ±492
2.5S2P	112 ±1.1	8.5 ±0.4	76.2 ±3.1	6654 ±714	2085 ±278
5S2P	117 ±1.3	7.4 ±0.3	77.4 ±3.7	8758 ±646	3323 ±283

CHAPTER 5. CONCLUSIONS AND FUTURE WORK

This work set out to approach improving S2 GFRPs through investigating the potential of glass fiber sizing modification and the effect of the addition of CNCs into the matrix. More specifically, the goal of this work has been to evaluate the possibility of improving the tensile and flexural strength and moduli without losing in impact properties. This chapter presents conclusions of this work as well as suggestions for future work.

5.1 Conclusions

In Chapter 3, composites with differently sized S2 glass fibers were manufactured and characterized. The sizing formulations were also compared using surface analysis techniques on the as-received fibers. It was observed that one of the glass fiber sizing formulations resulted in a 37% improvement in tensile strength over a differently sized S2 GF composite. That same composite (0S2P) also outperformed the least performing composite (0S2R) by 34% in flexural strength. Composite 0S2S outperformed 0S2R by 25% and 21% in the tensile and flexural moduli, respectively. Impact testing and the areas under the curve of tan δ reveal that no decrease in impact strength accompanied those improvements in flexural and tensile properties. This highlights the potential of sizing modification for improving the mechanical properties of S2 GFRPs.

The differently sized S2 glass fibers were also characterized to suggest some parameters that could be useful for the design of glass fiber sizing. Microscopy revealed that the highest performing composites had sizing films that are notably more conforming to the fiber surfaces. This increased conformability was interpreted to be an indication of

increased interfacial strength, which was underscored by the results of tensile and flexural tests. Analysis of the surface chemistry of the fibers revealed that the highest performing sizing formulations had the least amount of C-C single bonding, indicating more potential for compatible functional groups on the sizing. Additionally, these two sizing formulations (S2-S and S2-P) had the highest amount of oxygen atoms on the surface, this was also interpreted as increased potential for interactions between the fibers and the polyester matrix. Lastly, sizing coverage was not deemed to be essential, as sizing R had statistically lower amounts of Al atomic %, which indicated increased surface coverage, while it was expected that increased surface coverage of the sizing would result in improved mechanical properties, the increased potential for interactions between the other sizing formulations and the matrix resulted in surface coverage being less of a deciding factor.

In Chapter 4, CNCs were added into the polyester matrix in different concentrations. Both E-glass and S2-glass composites were manufactured and characterized. SEM was used to ensure that no large CNC agglomerates had formed. The addition of CNCs did not result in significant changes in tensile and flexural testing. Impact testing suggested that the addition of CNC results in an increase in impact strength, but differences were not statistically significant. Results of DMA testing did not reveal statistically different values for the moduli, but it was observed the glass transition temperature of the composite with 5 PHR resin was statistically higher than that of the 0 PHR resin. This was explained as the CNC whisker-shaped nanoparticles restricting the mobility of the matrix polymer chains. Lastly, the Halpin-Tsai and E_{random} equations were utilized to predict values of the tensile modulus of the different composites, and it

showed great potential for the addition of CNCs to S2 GFRPs in terms of increasing the tensile modulus of the composites.

Holistically, considering the demonstrated potential of sizing modification on mechanical properties, as well as the observed trend of impact strength increasing with the addition of CNCs and theoretical frameworks suggesting increased elastic modulus with the addition of CNCs leads to the conclusion that the most effective approach of improving the mechanical properties of composites is to exploit the structural hierarchy. This was done in this work by utilizing or modifying structural elements of different scales within the composite.

5.2 Future Work

Characterizing the sizing formulation in its liquid state would have opened additional avenues for the characterization of the sizing formulation. However, due to the proprietary nature of the sizing formulation, this step was not feasible in this work. Additional suggestions include running mechanical tests on single fibers to better compare the effect of the sizing on the mechanical behavior of the fibers. This work was chiefly concerned with SMC composites, and as such, single fiber tests were not employed.

Additionally, while the qualitative assessment of the conformability of the sizing films was beneficial in this study, a quantitative approach might be useful for future studies. Sageman-Furnas *et al.* proposed an approach that might be of great help in terms of quantifying the conformability of sizing films [78]. However, the model mentioned is suited for spherical coverages which wouldn't be ideal for the cylindrical geometry of the fibers.

Regarding the second portion of this work, it's recommended to attempt similar experiments with functionalized CNCs. CNCs could be functionalized to promote interactions with the matrix and the fibers, thus increasing the interfacial strength and consequently improving the mechanical properties of the composites. Additionally, the sizing formulation itself could be designed with CNCs in mind to promote interactions between the fiber sizing and the CNCs. Another suggestion for future work is to investigate various ways of incorporating CNCs into composites. More specifically, it's suggested to investigate the potential of adding CNCs onto the S2 glass fibers prior to composite manufacturing. This has been tried previously, but not with S2 glass fibers. Lastly, this work utilized the Halpin-Tsai equations, and while helpful, the model is idealistic, and it's suggested to employ more realistic models. Luo *et al.* suggested a modified Halpin-Tsai model that takes the nanoscale of additives into account [79].

REFERENCES

1. Seymour, R.B., R.D. Deanin, and A.C.S. Meeting, *History of Polymeric Composites*. 1987: Taylor & Francis.

2. Gupta, M., *Polymer composite*. 2007: New Age International.

3. Asadi, A., et al., *Improving the interfacial and mechanical properties of short glass fiber/epoxy composites by coating the glass fibers with cellulose nanocrystals.* eXPRESS Polymer Letters, 2016. **10**: p. 587-597.

4. *Chapter 6: Innovating Clean Energy Technologies in Advanced Manufacturing*, in *The Quadrennial Technology Review: An Assessment Of Energy Technologies And Research Opportunities*. 2015.

5. Güler, T., et al., *Lightweight design of an automobile hinge component using glass fiber polyamide composites.* Materials Testing, 2018. **60**(3): p. 306-310.

6. Callister, W.D., Jr. and D.G. Rethwisch, *Materials science and engineering : an introduction*. 7th edition / ed. 2010, Hoboken, NJ: John Wiley & Sons.

7. Clarkson, C.M., et al., *Recent Developments in Cellulose Nanomaterial Composites.* Advanced Materials, 2021. **33**(28): p. 2000718.

8. Mallick, P.K., *Thermoset–matrix composites for lightweight automotive structures*. 2010, Elsevier. p. 208-231.

9. Biron, M., *The Plastics Industry*. 2018, Elsevier. p. 31-132.

10. Dodiuk, H. and S.H. Goodman, *Handbook of Thermoset Plastics*. 2021, Burlington, UNITED STATES: Elsevier Science & Technology Books.

11. *AGY Advanced Materials Datasheet*.

12. Comte, E., et al., *Void formation and transport during SMC manufacturing: Effect of the glass fiber sizing.* Polymer Composites, 2006. **27**(3): p. 289-298.

13. Nicolais, L., *Wiley Encyclopedia of Composites.* 2011.

14. Thomason, J.L., *Glass fibre sizing: A review.* Composites Part A: Applied Science and Manufacturing, 2019. **127**.

15. Petersen, H.N., et al., *The influence of removing sizing on strength and stiffness of conventional and high modulus E-glass fibres.* IOP Conference Series: Materials Science and Engineering, 2016. **139**: p. 012040.

16. Thomason, J.L., *Glass fibre sizing: A review.* Composites Part A: Applied Science and Manufacturing, 2019. **127**: p. 105619.

17. Dey, M., et al., *Influence of sizing formulations on glass/epoxy interphase properties.* Composites Part A: Applied Science and Manufacturing, 2014. **63**: p. 59-67.

18. Feuillade, V., et al., *Relationships between the glass fibre sizing composition and the surface quality of sheet moulding compounds (SMC) body panels.* Composites Science and Technology, 2006. **66**(1): p. 115-127.

19. Mäder, E., et al., *Influence of an optimized interphase on the properties of polypropylene/glass fibre composites.* Composites Part A: Applied Science and Manufacturing, 1996. **27**(9): p. 907-912.

20. Ishida, H., *A review of recent progress in the studies of molecular and microstructure of coupling agents and their functions in composites, coatings and adhesive joints.* Polymer Composites, 1984. **5**(2): p. 101-123.

21. Klemm, D., et al., *Cellulose: Fascinating Biopolymer and Sustainable Raw Material.* Angewandte Chemie International Edition, 2005. **44**(22): p. 3358-3393.

22. Moon, R.J., et al., *Cellulose nanomaterials review: structure, properties and nanocomposites.* Chemical Society Reviews, 2011. **40**(7): p. 3941.

23. Foster, E.J., et al., *Current characterization methods for cellulose nanomaterials.* Chemical Society Reviews, 2018. **47**(8): p. 2609-2679.

24. Zhou, J., et al., *Synthesis of Multifunctional Cellulose Nanocrystals for Lectin Recognition and Bacterial Imaging.* Biomacromolecules, 2015. **16**(4): p. 1426-1432.

25. Bai, L., et al., *Comparison of Hydrophilicity and Mechanical Properties of Nanocomposite Membranes with Cellulose Nanocrystals and Carbon Nanotubes.* Environmental Science & Technology, 2017. **51**(1): p. 253-262.

26. Potter, K.A., et al., *Curcumin-releasing mechanically adaptive intracortical implants improve the proximal neuronal density and blood–brain barrier stability.* Acta Biomaterialia, 2014. **10**(5): p. 2209-2222.

27. Veigel, S., et al., *Particle Board and Oriented Strand Board Prepared with Nanocellulose-Reinforced Adhesive.* Journal of Nanomaterials, 2012. **2012**: p. 1-8.

28. Haque, E., et al., *Scalable coating methods for enhancing glass fiber–epoxy interactions with cellulose nanocrystals.* Cellulose, 2021. **28**(8): p. 4685-4700.

29. Diloreto, E., et al., *Freeze dried cellulose nanocrystal reinforced unsaturated polyester composites: challenges and potential.* Cellulose, 2019. **26**(7): p. 4391-4403.

30. George, J. and S. S N, *Cellulose nanocrystals: synthesis, functional properties, and applications.* Nanotechnology, Science and Applications, 2015: p. 45.

31. Beck-Candanedo, S., M. Roman, and D.G. Gray, *Effect of Reaction Conditions on the Properties and Behavior of Wood Cellulose Nanocrystal Suspensions.* Biomacromolecules, 2005. **6**(2): p. 1048-1054.

32. Vanderfleet, O.M. and E.D. Cranston, *Production routes to tailor the performance of cellulose nanocrystals.* Nature Reviews Materials, 2021. **6**(2): p. 124-144.

33. Moon, R.J., G.T. Schueneman, and J. Simonsen, *Overview of Cellulose Nanomaterials, Their Capabilities and Applications.* JOM, 2016. **68**(9): p. 2383-2394.

34. Habibi, Y., L.A. Lucia, and O.J. Rojas, *Cellulose Nanocrystals: Chemistry, Self-Assembly, and Applications.* Chemical Reviews, 2010. **110**(6): p. 3479-3500.

35. Posteck, M.T., et al., *Production and Applications of Cellulose Nanomaterials*. 2013.

36. Dufresne, A., J.-Y. Cavaillé, and M.R. Vignon, *Mechanical behavior of sheets prepared from sugar beet cellulose microfibrils.* Journal of Applied Polymer Science, 1997. **64**(6): p. 1185-1194.

37. Hanley, S.J., et al., Cellulose, 1997. **4**(3): p. 209-220.

38. Ogawa, Y. and J.-L. Putaux, *Transmission electron microscopy of cellulose. Part 2: technical and practical aspects.* Cellulose, 2019. **26**(1): p. 17-34.

39. Ifuku, S., et al., *Surface Modification of Bacterial Cellulose Nanofibers for Property Enhancement of Optically Transparent Composites: Dependence on Acetyl-Group DS.* Biomacromolecules, 2007. **8**(6): p. 1973-1978.

40. Singletary, J., *Transverse compression of PPTA fibers.* Mechanics of Composite Materials, 2000. **36**(4): p. 319-326.

41. Yu, M., *Strength and Breaking Mechanism of Multiwalled Carbon Nanotubes Under Tensile Load.* Science, 2000. **287**(5453): p. 637-640.

42. Callister, W.D., *Materials science and engineering : an introduction*. Ninth edition / William D. Callister, Jr. Department Of Metallurgical Engineering, the University

Of Utah, David G. Rethwisch, Department of Chemical and Biochemical Engineering, the University of Iowa.. ed, ed. D.G. Rethwisch. 2014: Hoboken, NJ : John Wiley and Sons, Inc.

43. Asadi, A., et al., *Lightweight sheet molding compound (SMC) composites containing cellulose nanocrystals.* Composite Structures, 2017. **160**: p. 211-219.

44. Rosato, D.V. and D.V. Rosato, *Chapter 6 - Markets/Products*, in *Reinforced Plastics Handbook (Third Edition)*, D.V. Rosato and D.V. Rosato, Editors. 2005, Elsevier Science: Amsterdam. p. 483-612.

45. Baaij, S. and F. Johannes, *Advances In Sheet Molding Compounds For Automotive Applications*, in *Mechanical Engineering*. 2018, Georgia Institute of Technology : Atlanta, Georgia.

46. Mazumdar, S.K., *Composites manufacturing : materials, product, and process engineering*. 2002: Boca Raton, Fla. : CRC Press.

47. Park, C.H. and W.I. Lee, *3 - Compression molding in polymer matrix composites*, in *Manufacturing Techniques for Polymer Matrix Composites (PMCs)*, S.G. Advani and K.-T. Hsiao, Editors. 2012, Woodhead Publishing. p. 47-94.

48. Rosato, D.V. and D.V. Rosato, *Chapter 10 - Summary*, in *Reinforced Plastics Handbook (Third Edition)*, D.V. Rosato and D.V. Rosato, Editors. 2005, Elsevier Science: Amsterdam. p. 997-1034.

49. Rosato, D.V. and D.V. Rosato, *Chapter 4 - Compound constructions*, in *Reinforced Plastics Handbook (Third Edition)*, D.V. Rosato and D.V. Rosato, Editors. 2005, Elsevier Science: Amsterdam. p. 212-253.

50. Damron, S., *Discussion on S2 GF and Sizing*. 2021.

51. Hojabr, S., *NCC® NCV100-NASD90 Certificate of Analysis*. 2020, CelluForce: Windsor, Québec, Canada.

52. *Standard Practices for Force Verification of Testing Machines*.

53. *Standard Test Method for Tensile Properties of Plastics*.

54. *Standard Practice for Verification and Classification of Extensometer Systems*.

55. *Standard Test Methods for Flexural Properties of Unreinforced and Reinforced Plastics and Electrical Insulating Materials*.

56. *Standard Test Method for Unnotched Cantilever Beam Impact Resistance of Plastics*.

57. *Standard Test Method for Determining the Charpy Impact Resistance of Notched Specimens of Plastics*.

58. *Standard Test Methods for Density and Specific Gravity (Relative Density) of Plastics by Displacement*.

59. *Standard Test Method for Ignition Loss of Cured Reinforced Resins*.

60. *Standard Practice for Plastics: Dynamic Mechanical Properties: Determination and Report of Procedures*.

61. Young, C. *Predicting Practical Properties of Unfilled and Filled Adhesives From Thermomechanical Data*. 2011.

62. *Standard Test Methods for Void Content of Reinforced Plastics*.

63. Callister, W.D. and D.G. Rethwisch, *Materials Science and Engineering: An Introduction*. 2018: Wiley.

64. Dekkers, M.E.J. and D. Heikens, *The effect of interfacial adhesion on the tensile behavior of polystyrene–glass-bead composites.* Journal of Applied Polymer Science, 1983. **28**(12): p. 3809-3815.

65. Lee, D.G. and S.S. Cheon, *Impact Characteristics of Glass Fiber Composites with Respect to Fiber Volume Fraction.* Journal of Composite Materials, 2001. **35**(1): p. 27-56.

66. Novak, R.C. and M.A. DeCrescente, *Impact Behavior of Unidirectional Resin Matrix Composites Tested in the Fiber Direction*, H.T. Corten, Editor. 1972, ASTM International: West Conshohocken, PA. p. 311-323.

67. Beaumont, P.W.R., *A Fracture Mechanics Approach to Failure in Fibrous Composites.* The Journal of Adhesion, 1974. **6**(1-2): p. 107-137.

68. Mallick, P.K., *Fiber-Reinforced Composites.* 2007.

69. Stevie, F.A. and C.L. Donley, *Introduction to x-ray photoelectron spectroscopy.* Journal of Vacuum Science & Technology A, 2020. **38**(6): p. 063204.

70. Affdl, J.C.H. and J.L. Kardos, *The Halpin-Tsai equations: A review.* Polymer Engineering & Science, 1976. **16**(5): p. 344-352.

71. Mallick, P.K., *Appendixes*. 2008, Taylor & Francis. p. 1-1.

72. *AGY ADVANTEX® Generic Glass Fiber*. [cited 2021; Available from: http://www.matweb.com/search/DataSheet.aspx?MatGUID=0f865acae7cb4042af71ebbe5a1ba78e&ckck=1.

73. Bergenstråhle, M., L.A. Berglund, and K. Mazeau, *Thermal Response in Crystalline Iβ Cellulose: A Molecular Dynamics Study.* The Journal of Physical Chemistry B, 2007. **111**(30): p. 9138-9145.

74. *Pultru® Multi-Purpose Isophthalic Polyester Resin*.

75. Visakh, P.M., et al., *Crosslinked natural rubber nanocomposites reinforced with cellulose whiskers isolated from bamboo waste: Processing and mechanical/thermal properties.* Composites Part A: Applied Science and Manufacturing, 2012. **43**(4): p. 735-741.

76. Cao, X., H. Dong, and C.M. Li, *New Nanocomposite Materials Reinforced with Flax Cellulose Nanocrystals in Waterborne Polyurethane.* Biomacromolecules, 2007. **8**(3): p. 899-904.

77. Petersson, L., I. Kvien, and K. Oksman, *Structure and thermal properties of poly(lactic acid)/cellulose whiskers nanocomposite materials.* Composites Science and Technology, 2007. **67**(11-12): p. 2535-2544.

78. Sageman-Furnas, A.O., et al., *The Sphereprint: An approach to quantifying the conformability of flexible materials.* Textile Research Journal, 2014. **84**(8): p. 793-807.

79. Luo, Z., et al., *Modified rule of mixtures and Halpin–Tsai model for prediction of tensile strength of micron-sized reinforced composites and Young's modulus of multiscale reinforced composites for direct extrusion fabrication.* Advances in Mechanical Engineering, 2018. **10**(7): p. 168781401878528.